Remote Sensing of Environment 247 (2020) 111935

Contents lists available at ScienceDirect

Remote Sensing of Environment

journal homepage: www.elsevier.com/locate/rse

# Evaluation of global leaf area index and fraction of absorbed photosynthetically active radiation products over North America using Copernicus Ground Based Observations for Validation data

Luke A. Brown[a,*], Courtney Meier[b], Harry Morris[a], Julio Pastor-Guzman[a], Gabriele Bai[c], Christophe Lerebourg[c], Nadine Gobron[d], Christian Lanconelli[d], Marco Clerici[d], Jadunandan Dash[a]

[a] School of Geography and Environmental Science, University of Southampton, Highfield, Southampton SO17 1BJ, United Kingdom
[b] National Ecological Observatory Network, Boulder, CO 80301, United States
[c] ACRI-ST, 06904 Sophia-Antipolis, France
[d] European Commission Joint Research Centre, 21027 Ispra, Italy

ARTICLE INFO

*Keywords:*
Copernicus
digital hemispherical photography
FAPAR
GBOV
LAI
MODIS
PROBA-V
validation
VIIRS

ABSTRACT

With a growing number of Earth observation (EO) products available through operational programmes such as the European Union's Copernicus, there is increasing emphasis on product accuracy and uncertainty, necessitating evaluation against in situ reference measurements. Whilst existing reference datasets have proven a valuable resource, they incorporate little data with which products from recent EO instruments can be assessed. A reliance on individual field campaigns has also led to several inconsistencies, whilst limiting the extent to which temporal variations in EO product performance can be captured. Recently established environmental monitoring networks such as the National Ecological Observatory Network (NEON), which collect routine in situ measurements using standardised instruments and protocols, provide a promising opportunity in this respect. The Copernicus Ground Based Observations for Validation (GBOV) service was initiated in recognition of this fact. In the first component of the project, raw observations from existing networks have been collected and processed to provide reference data for a range of EO land products. In this study, we focus on leaf area index (LAI) and the fraction of absorbed photosynthetically active radiation (FAPAR). Raw digital hemispherical photography (DHP) from twenty NEON sites was processed to derive in situ reference measurements, which were then upscaled to provide high spatial resolution reference maps. Using these data, we assess the recently released Copernicus Global Land Service (CGLS) 300 m Version 1 (V1) products derived from PROBA-V, in addition to existing products derived from the Moderate Resolution Imaging Spectroradiometer (MODIS) and Visible Infrared Radiometer Suite (VIIRS). When evaluated against reference data, the CGLS 300 m V1 product demonstrated the best agreement (RMSD = 0.57 for LAI and 0.08 for FAPAR), followed by the Collection 6 VNP15A2H and MOD15A2H products (RMSD = 0.81 to 0.89 for LAI and 0.12 for FAPAR). Differing assumptions of the products and in situ reference measurements, which cause them to be sensitive to slightly different quantities, are thought to explain apparent biases over sparse vegetation and forest environments. To ensure their continued utility, future work should focus on updating the GBOV in situ reference measurements, implementing additional corrections, and improving their geographical representativeness.

## 1. Introduction

With repeat and systematic global coverage, Earth observation (EO) data provide a unique opportunity to monitor vegetation biophysical variables such as leaf area index (LAI) and the fraction of absorbed photosynthetically active radiation (FAPAR). Both LAI and FAPAR have been designated essential climate variables by the Global Climate Observing System (GCOS, 2019), as they are key inputs in a range of applications including climate modelling, numerical weather prediction, understanding biosphere-atmosphere interactions, and agricultural and forest monitoring (Ogutu et al., 2013; Richardson et al., 2013; Sellers et al., 1997). A range of global LAI and FAPAR products

* Corresponding author.
*E-mail address:* l.a.brown@soton.ac.uk (L.A. Brown).

https://doi.org/10.1016/j.rse.2020.111935
Received 9 January 2020; Received in revised form 4 May 2020; Accepted 30 May 2020
Available online 23 June 2020

have been produced operationally over the last two decades, primarily utilising data from optical instruments on-board EO satellites. The underlying algorithms used to generate such products include retrieval techniques such as radiative transfer model (RTM) inversion, statistical retrieval, and hybrid approaches (Baret and Buis, 2008; Verrelst et al., 2015). Current examples of moderate spatial resolution (i.e. 300 m to 500 m) LAI and FAPAR products include those derived from the Moderate Resolution Imaging Spectroradiometer (MODIS) (Yan et al., 2016a), Visible Infrared Radiometer Suite (VIIRS) (Yan et al., 2018), Ocean and Land Colour Instrument (OLCI) (Gobron, 2010), VEGETATION (VGT), and PROBA-V (Lacaze et al., 2015).

Users now have access to a growing number of EO products, made routinely available through dedicated operational programmes such as the European Union's Copernicus. Due to their operational nature and a growing user base, there is increasing emphasis on product accuracy and quantifying uncertainty; routine and systematic product evaluation is now an essential part of the EO data production and delivery process. Whilst intercomparison of EO products can provide potentially useful information on their consistency, evaluation against independent in situ reference measurements is necessary to effectively quantify product accuracy. Such assessments are critical if EO products are to be used in data assimilation schemes, which require quantitative estimates of parameter uncertainty. In light of the importance of these activities, international initiatives such as the Committee on Earth Observation Satellites (CEOS) Working Group on Calibration and Validation (WGCV) and Quality Assurance Framework for Earth Observation (QA4EO) have been working with the community to develop best practices and protocols for evaluation of EO derived products. Similarly, recognising the need for product evaluation, data providers such as the European Space Agency (ESA) have recently established a series of projects focussed solely on fiducial reference measurements (ESA, 2019).

The Land Product Validation (LPV) sub-group of the CEOS WGCV defines a four-stage hierarchy for EO product evaluation, through which EO products should progress. Several currently operational LAI and FAPAR products have reached stage two of this hierarchy, which states that 'product accuracy is assessed over a significant set of locations and time periods' (Fernandes et al., 2014). An overview of the products considered in this study and their evaluation status is provided in Section 2. Previous evaluation exercises have demonstrated that the majority of products are characterised by consistent seasonality, but demonstrate discrepancies in magnitude, owing to the differing assumptions of their respective retrieval algorithms (Camacho et al., 2013; Tao et al., 2015; Weiss et al., 2014; Yan et al., 2016b). So far, progress towards the third stage of the CEOS WGCV LPV hierarchy has been restricted by in situ reference measurement datasets that are both spatially and temporally limited.

In terms of vegetation biophysical variables, the DIRECT 2.0 database, which is maintained by the CEOS WGCV LPV sub-group, is currently the largest collection of in situ reference measurements available for evaluating moderate spatial resolution LAI and FAPAR products (CEOS WGCV LPV, 2017). The database contains 242 samples collected over 140 sites between 2000 and 2017, and features data collected during numerous field campaigns carried out under the BigFoot (Cohen and Justice, 1999), Southern African Regional Science Initiative (SAFARI-2000) (Swap and Privette, 1999), Validation of Land European Remote Sensing Instruments (VALERI) (Baret et al., 2005), and Implementation of Multiscale Agricultural Indicators Exploiting Sentinels (ImagineS) (ImagineS Consortium, 2016) projects, in addition to efforts by Boston University (Yang et al., 2006), the University of Alberta, Canada Centre for Remote Sensing (CCRS) (Abuelgasim et al., 2006), Earth Observation Laboratory (EOLAB), Environmental Protection Agency (EPA) (Iiames et al., 2004), and ESA (CEOS WGCV LPV, 2017).

Datasets included within the DIRECT 2.0 database have proven to be a valuable resource for EO product evaluation (Bacour et al., 2006; Camacho et al., 2013; Garrigues et al., 2008a; Weiss et al., 2007, 2014; Yan et al., 2016b). However, because individual field campaigns have been carried out by different groups using a range of instruments and data collection protocols, they are subject to a number of inconsistencies (Camacho et al., 2013; Garrigues et al., 2008a; Yan et al., 2016b). Examples include:

- Forest sites at which the understory is not characterised;
- The use of instruments that cannot account for the effects of foliage clumping, and therefore only enable quantification of effective LAI ($LAI_e$).

Indeed, in a recent review of LAI products and evaluation efforts, Fang et al. (2019a) identified the need for standardisation of field measurements. Additionally, due to a reliance on individual field campaigns, few sites within the database feature data collected throughout the phenological cycle or over a continuous period of multiple years. Most field campaigns have been conducted on a one-off basis during the peak of the growing season, limiting the extent to which temporal variations in EO product performance can be captured (Camacho et al., 2013; Fang et al., 2019a; Garrigues et al., 2008a; Weiss et al., 2014; Yan et al., 2016b). This is one factor that restricts progress towards the third stage of the CEOS WGCV LPV hierarchy, which states that product accuracy should be 'assessed in a statistically robust way over multiple locations and time periods' (Fernandes et al., 2014). Finally, the majority of the data are historical, so the database has a limited number of points with which products from recent sensors such as VIIRS, PROBA-V and OLCI can be assessed.

In parallel to activities focussed solely on the evaluation of EO products, several broader environmental monitoring networks have been established over the last decade, focussing on the provision of continuous, long-term ecological and environmental data across permanent measurement sites. Examples include the National Ecological Observatory Network (NEON) in the United States (Kao et al., 2012), the Terrestrial Ecosystem Research Network (TERN) in Australia (Karan et al., 2016), and the Integrated Carbon Observation System (ICOS) in Europe (Gielen et al., 2018). Many of these networks feature a free and open data policy, and as they move into routine operations, several are planning or already performing regular in situ measurements of vegetation biophysical variables including LAI and FAPAR (amongst a host of other environmental indicators). Importantly, because these networks are centrally coordinated, they also benefit from the use of instruments and data collection protocols that are standardised across sites.

Recognising the need for EO product quality assurance, the limitations of existing reference datasets, and the opportunities provided by new and existing environmental monitoring networks, the European Commission recently initiated the Ground Based Observations for Validation (GBOV) service. As part of the Copernicus Global Land Service (CGLS), the aim of GBOV is to provide consistent, continuous, and quality controlled in situ reference measurements for evaluation of EO derived land products. In its first component, raw observations from a range of existing networks have been collected and processed to provide datasets suitable for evaluating surface albedo, land surface temperature, soil moisture, and vegetation products. These data are freely available to the community via the GBOV website (https://land.copernicus.eu/global/gbov/). By exploiting data from networks operating standardised protocols and applying a common data processing chain, the GBOV service is designed to avoid the inconsistencies associated with previous in situ reference measurement datasets. Additionally, the data provided by GBOV must conform to minimum requirements on temporal frequency and coverage, ensuring the service is useful for assessing temporal variations in the performance of currently operational EO products. This paper focuses specifically on the in situ reference measurements related to LAI and FAPAR, and has three objectives:

**Table 1**
Major characteristics of the three EO products considered within the study.

| Product | Instrument | Spatial resolution (m) | Temporal resolution (days) | Temporal coverage | Retrieval approach | Evaluation status | Reference |
|---|---|---|---|---|---|---|---|
| CGLS 300 m V1 | PROBA-V | 300 | 10 | 2014 to Present | ANN trained with CYCLOPES and Collection 5 MOD15A2 products | Stage 1 | Lacaze et al. (2015) |
| MOD15A2H | MODIS | 500 | 8 | 2002 to Present | LUT inversion of a three-dimensional RTM | Stage 2 | Yan et al., 2016a |
| VNP15A2H | VIIRS | 500 | 8 | 2012 to Present | LUT inversion of a three-dimensional RTM | Stage 1 | Yan et al. (2018) |

1. To present the data and algorithms used to derive the GBOV in situ reference measurements;
2. To evaluate the impact of neglecting the understory layer when performing in situ measurements in forest environments;
3. To assess the performance of the recently released CGLS 300 m Version 1 (V1) products derived from PROBA-V and existing products derived from MODIS and VIIRS through evaluation against upscaled in situ reference measurements and product intercomparison.

## 2. EO derived LAI and FAPAR products

In this section, the major characteristics of the three EO products considered within the paper are provided (Table 1). We restricted our analysis to currently operational products providing moderate spatial resolution (i.e. 300 m to 500 m) estimates of LAI and FAPAR at the global scale. Although other products are available, they were not considered here because they are either a) no longer being produced, or b) produced at a spatial resolution that greatly exceeds GCOS (2019) requirements (250 m for LAI and 500 m for FAPAR). For example, the CYCLOPES and Global Land Surface Satellite (GLASS) product archives extend only to 2008 and 2017, respectively, and whilst operational products are delivered by the European Organization for the Exploitation of Meteorological Satellites (EUMETSAT) Land Surface Analysis Satellite Application Facility (LSA SAF), they are provided at a spatial resolution of 1.1 km to 4.8 km.

### 2.1. CGLS 300 m V1 LAI and FAPAR

The CGLS 300 m V1 LAI and FAPAR products, which are derived from PROBA-V, cover the period from January 2014 to present (Lacaze et al., 2015). They are delivered every ten days. 1 km spatial resolution products are also available from the CGLS, making use of the GEOV1 and GEOV2 algorithms and data from the VGT instrument to extend coverage back to 1999 (Baret et al., 2013; Verger et al., 2014). In this paper, we focus on the 300 m V1 products, which were released in, 2017, and are based on the so-called GEOV3 algorithm (Baret et al., 2016).

Like its predecessors, the GEOV3 algorithm aims to exploit the strengths of other established EO products to provide improved estimates of LAI and FAPAR. This is achieved by training an artificial neural network (ANN) with red and near-infrared surface reflectance values (and their associated viewing and illumination geometries), in addition to a weighted average of contemporaneous LAI and FAPAR estimates from CYCLOPES (Baret et al., 2007) and the Collection 5 MOD15A2 product (Yang et al., 2006). Whilst CYCLOPES is known to saturate at high LAI and FAPAR values (Garrigues et al., 2008a; Weiss et al., 2007), the Collection 5 MOD15A2 product is known to overestimate lower LAI and FAPAR values (Baret et al., 2013). By preferentially weighting low CYCLOPES and high MOD15A2 values, the algorithm attempts to reduce these issues. After application of the ANN to derive instantaneous values, temporal compositing, smoothing, and gap filling procedures are applied. As comparatively little evaluation has been performed on the CGLS 300 m V1 products, the data provider currently considers them to be in their demonstration stage (CGLS, 2017). A recent evaluation was carried out by Fuster et al. (2020) over cultivated crops, who concluded that the products provide good precision and smooth temporal profiles, but demonstrate positive biases for both LAI and FAPAR.

### 2.2. Collection 6 MOD15A2H LAI and FAPAR

The Collection 6 MOD15A2H product (Myneni et al., 2015; ORNL DAAC, 2018) is derived from the MODIS instrument on-board Terra, and provides estimates of LAI and FAPAR at a spatial resolution of 500 m, covering the period from 2002 to present (Yan et al., 2016a). Data

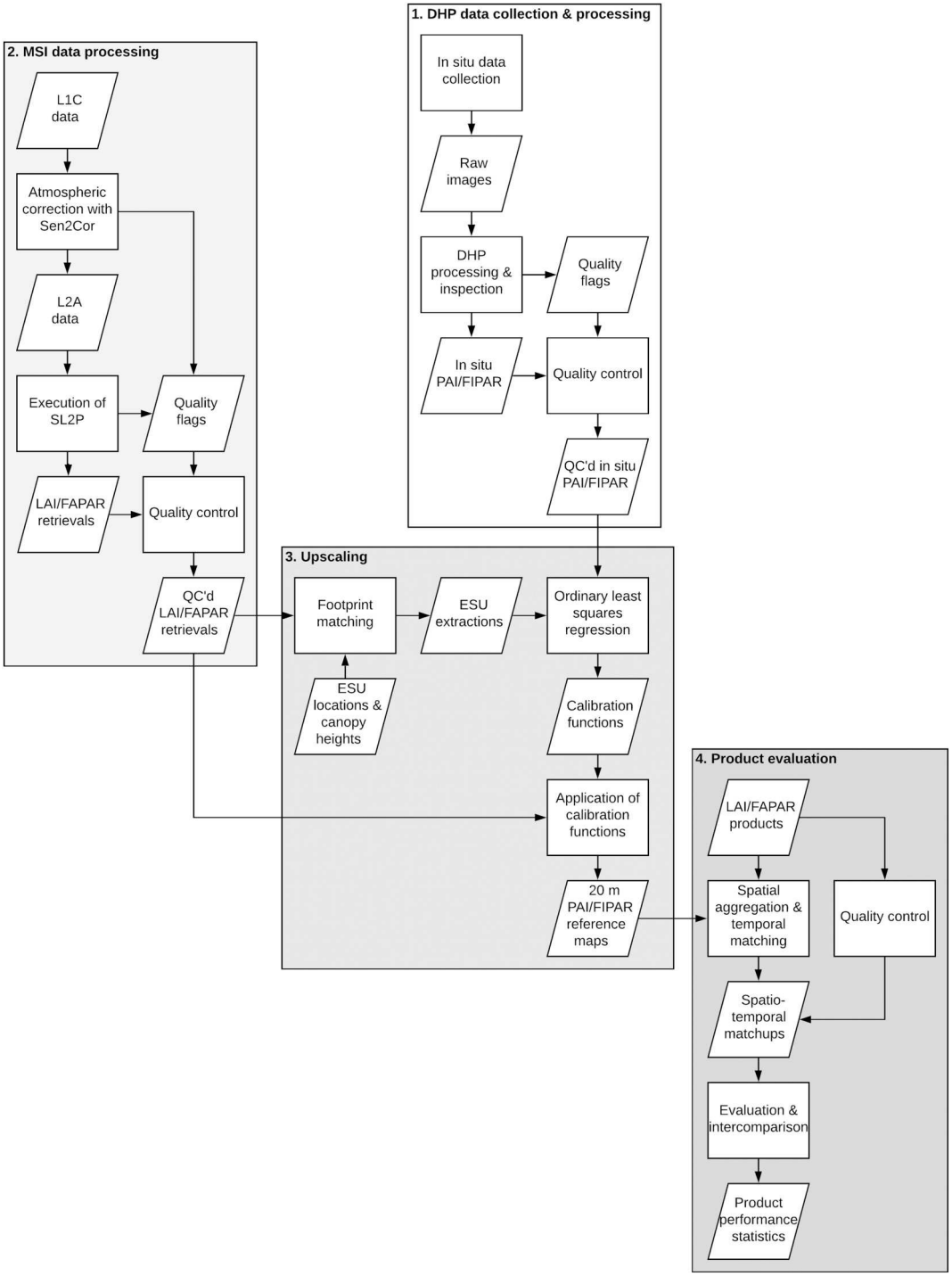


**Fig. 1.** Flow diagram providing an overview of the product evaluation methodology.

are delivered every eight days. Related products include MYD15A2H, which is produced from the MODIS instrument on-board Aqua, and the MCD15A2H product, which combines data from the instruments on-board both Aqua and Terra. A final product, MCD15A3H, exploits the additional acquisitions of this combined dataset to increase the temporal resolution to four days. In this paper, we focus on the MOD15A2H product, as when compared to Aqua, the earlier overpass time of Terra reduces cloud contamination and better matches that of the other investigated products (Yan et al., 2016b).

The Collection 6 MOD15A2H algorithm is based on three-dimensional RTM inversion, making use of biome-specific look up tables (LUTs), which are selected according to an eight-biome land cover map. Retrieval is achieved by comparing observed red and near-infrared surface reflectance values (and their uncertainties and associated viewing and illumination geometries) with the modelled values stored in the LUT. Observed and modelled values that differ by less than a biome-specific threshold are considered acceptable solutions, and the mean and standard deviation of the associated LAI and FAPAR values from the LUT are reported. If no acceptable solutions exist, a back-up statistical retrieval algorithm is triggered, which is based on biome-specific relationships between the Normalised Difference Vegetation Index (NDVI) and LAI/FAPAR. Within the eight day compositing window, the observation with the highest FAPAR value is selected, following the maximum value compositing (MVC) approach (Yan et al.,

2016a).

When compared to the 1 km Collection 5 MOD15A2 product, the Collection 6 MOD15A2H product benefits from new 500 m MOD09GA surface reflectance and 500 m MCD12Q1 multi-year land cover inputs (Yan et al., 2016a). The product was released in 2015, and subsequent evaluation efforts have enabled it to reach stage two of the CEOS WGCV LPV hierarchy (Yan et al., 2016b). These efforts have demonstrated a) MOD15A2H LAI estimates are closer to LAI rather than $LAI_e$, b) improved performance when compared to the Collection 5 MOD15A2 product, and c) overestimation of FAPAR over sparse vegetation canopies (Yan et al., 2016b).

### 2.3. VNP15A2H V1 LAI and FAPAR

The VNP15A2H V1 product (Myneni and Knyazikhin, 2018; ORNL DAAC, 2018) is derived from the VIIRS instrument on-board the Suomi National Polar Orbiting Partnership (S-NPP) platform (Yan et al., 2018). Based on the same retrieval scheme as the Collection 6 MOD15A2H product, it is designed to provide continuity to the archive established by the MODIS instruments, which are now operating well beyond their design lives. Like MOD15A2H, the VNP15A2H product is provided at a spatial resolution of 500 m and a temporal resolution of eight days. It covers the period from 2012 to present, and has reached stage one of the CEOS WGCV LPV hierarchy, which states that product accuracy is assessed over a small set of locations and time periods. These efforts have demonstrated good agreement with limited in situ reference data, in addition to very good consistency with respect to the MOD15A2H product (NASA, 2017).

## 3. Materials and methods

### 3.1. Overview of product evaluation methodology

To assess the considered products, an evaluation methodology based on the two-stage approach recommended by the CEOS WGCV LPV sub-group was adopted (Fernandes et al., 2014; Morisette et al., 2006). In this approach, individual in situ reference measurements are performed within elementary sampling units (ESUs) that approximate the extent of one or more pixels of high spatial resolution imagery. By relating the in situ reference measurements at the ESU level with the spectral information in the high spatial resolution imagery, a high spatial resolution reference map can be produced. Finally, this reference map can be aggregated to the moderate spatial resolution of the product of interest to enable comparison. An overview of the product evaluation methodology is provided in Fig. 1.

### 3.2. Study sites

Of the existing environmental monitoring networks, one of the most mature in terms of data availability is NEON, which operates forty-seven terrestrial sites spread throughout the continental United States, Alaska, Hawaii, and Puerto Rico, covering twenty eco-climatic domains. For the first component of the GBOV project, twenty NEON sites were selected (Fig. 2 and Table 2), based on the availability of in situ reference measurements suitable for deriving LAI and FAPAR. These sites cover a wide range of vegetation types, including cultivated crops, deciduous broadleaf, evergreen broadleaf, and evergreen needleleaf forest, grassland/herbaceous vegetation, mixed forest, pasture/hay, shrub/scrub, and woody wetlands. Although the majority of NEON sites did not enter routine operations until 2017, at many sites data collection was carried out for several years prior to this (in some cases since 2013). Sites with a longer record of data collection were prioritised for inclusion in our analysis, in order to maximise the number of multi-year observations available for EO product evaluation. An analysis of site spatial representativeness is provided in Appendix A.

### 3.3. In situ reference measurements

Of particular utility for deriving in situ reference measurements of LAI and FAPAR is digital hemispherical photography (DHP), which, because of its efficiency and versatility, has proven to be a popular technique for sampling vegetation biophysical variables. Importantly, DHP enables the effects of foliage clumping to be accounted for, enabling quantification of both $LAI_e$ and LAI. Additionally, above canopy measurements (which are often impractical in forest canopies) are not a necessity, whilst downwards-facing images can be acquired to assess short or understory canopies. When compared to other passive techniques such as ceptometers and the LI-COR LAI-2000 instrument, Garrigues et al. (2008b) concluded that DHP was the most robust and least sensitive to illumination conditions, although it is worth noting that recent work has demonstrated the advantages of active methods such as terrestrial laser scanning (TLS) in this respect (Calders et al., 2018). Nevertheless, DHP remains a cost-effective option, and in recent years, further advances in image acquisition and pre-processing techniques have been made (Beckschäfer et al., 2013; Glatthorn and Beckschäfer, 2014; Macfarlane et al., 2014; Origo et al., 2017; Pueschel et al., 2012). At each NEON site, DHP data are collected at multiple plots every two weeks from leaf-out through to the end of senescence.

Although not explicitly designed for EO product evaluation, the DHP data collection protocol adopted by NEON is ideally suited to the two-stage approach recommended by the CEOS WGCV LPV sub-group. DHP data are collected within plots with a nominal extent of 20 m x 20 m, closely matching the spatial resolution of the Sentinel-2 Multispectral Instrument (MSI) data available for upscaling. Using a Nikon digital single lens reflex (DSLR) camera (models D750, D800 or D810) equipped with a full-frame fisheye lens (AF Fisheye-Nikkor 16mm f/2.8D), images are acquired at twelve points arranged in a cross pattern (Fig. 3). This corresponds to one of several within ESU sampling schemes widely used in EO product evaluation and recommended both by the CEOS WGCV LPV sub-group (Fernandes et al., 2014; Morisette et al., 2006) and within the VALERI project (Baret et al., 2005). Where an understory and overstory is present, images are acquired in both upwards- and downwards-facing directions. Further information on the NEON DHP acquisition protocol is provided by Meier et al. (2018).

When estimating LAI using optical techniques, an important consideration is the influence of woody material, particularly in forest environments. If woody area is not accounted for, then only measurements of plant area index (PAI) can be derived (Bréda, 2003; Jonckheere et al., 2004; Weiss et al., 2004; Yan et al., 2019). Given adequate contrast, it is possible to distinguish between foliage and other canopy elements such as stems and branches using DHP, enabling woody area to be corrected for (Woodgate et al., 2016). In the case of deciduous species, leaf-off measurements can also be used. Unfortunately, very little contrast between foliage and other canopy elements was observed in the NEON DHP data, which were optimally exposed for accurate estimation of gap fraction, whilst sampling during leaf-off conditions was not carried out. Because site-specific corrections for woody area could not be applied, as in many previous EO product evaluation exercises (Camacho et al., 2013; De Kauwe et al., 2011; Fang et al., 2019b; Heiskanen et al., 2012; Verger et al., 2011; Yin et al., 2017), we used PAI as a proxy for LAI.

In terms of FAPAR, it is important to note that only the fraction of intercepted photosynthetically active radiation (FIPAR) can be derived from DHP, but that because of strong absorption by photosynthetic pigments, the difference between FAPAR and FIPAR is considered marginal (Li et al., 2015; Weiss et al., 2014). For example, Gobron et al. (2006) demonstrated that whilst differences of up to 0.1 can occur over very bright backgrounds (i.e. snow), differences can be neglected in the overall FAPAR uncertainty budget under usual conditions (i.e. where a vegetated understory is present). Further details on the derivation of both PAI and FIPAR, including the corrections applied to account for foliage clumping in the case of PAI, are provided in Appendix B.

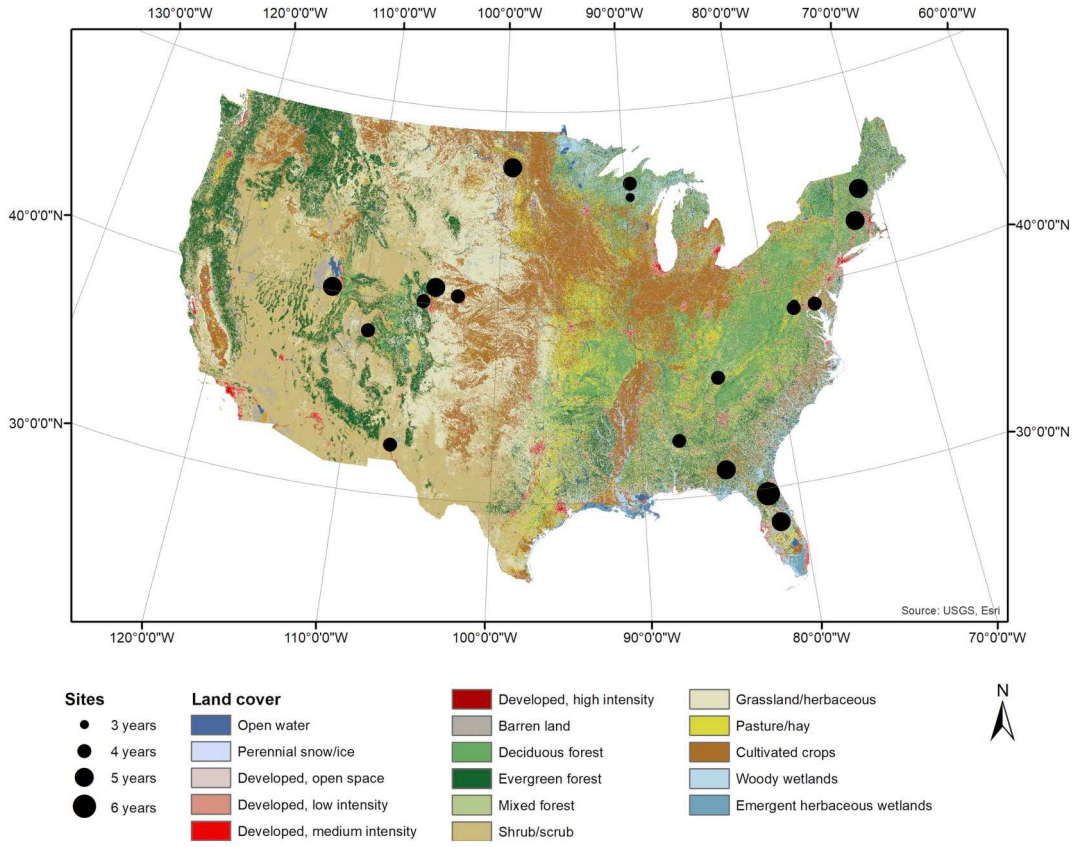


**Fig. 2.** NEON sites within the conterminous United States selected for the GBOV project. The size of the circles corresponds to the number of years of in situ data available at each site. Land cover data from the 2016 National Land Cover Database (NLCD) (Homer et al., 2020).

### *3.4. Evaluating the impact of neglecting the understory layer in forest environments*

Because DHP images were acquired in both upwards- and downwards-facing directions, our dataset provided an ideal opportunity to evaluate the impact of neglecting the understory layer when performing in situ reference measurements in forest environments. To quantify this impact, estimates of total PAI and FIPAR were compared with PAI and FIPAR derived using upwards-facing images only. The analysis was conducted on the in situ reference measurements from all forest and woody wetland sites, using the metrics described in Section 3.7.

### *3.5. Upscaling in situ reference measurements using Sentinel-2 MSI data*

To upscale the DHP-derived in situ reference measurements for evaluation of moderate spatial resolution EO products, high spatial

**Table 2**
NEON sites selected for the first phase of the GBOV project. Land cover data from the 2016 NLCD (Homer et al., 2020), with the exception of GUAN, where data are only available from the 2001 NLCD. Note that we further divided the NLCD deciduous and evergreen forest classes into broadleaf and needleleaf sub-classes.

| Site | Code | Dominant land cover (1.5 km x 1.5 km) | Mean canopy height (m) | Latitude | Longitude | In situ data availability |
|---|---|---|---|---|---|---|
| Bartlett Experimental Forest | BART | Mixed forest | 23.0 | 44.0639 | -71.2873 | 2014 to 2018 |
| Blandy Experimental Farm | BLAN | Pasture/hay | 1.0 | 39.0603 | -78.0716 | 2016 to 2018 |
| Central Plains Experimental Range | CPER | Grassland/herbaceous | 0.4 | 40.8155 | -104.7460 | 2014 to 2018 |
| Disney Wilderness Preserve | DSNY | Woody wetlands | 1.5 | 28.1250 | -81.4362 | 2014 to 2018 |
| Guanica Forest | GUAN | Evergreen broadleaf | 10.0 | 17.9696 | -66.8687 | 2015 to 2018 |
| Harvard Forest | HARV | Mixed forest | 26.0 | 42.5369 | -72.1727 | 2014 to 2018 |
| Jones Ecological Research Center | JERC | Evergreen needleleaf | 27.0 | 31.1948 | -84.4686 | 2014 to 2018 |
| Jornada | JORN | Shrub/scrub | 0.4 | 32.5907 | -106.8430 | 2015 to 2018 |
| Moab | MOAB | Shrub/scrub | 0.2 | 38.2483 | -109.3880 | 2015 to 2018 |
| Niwot Ridge Mountain Research Station | NIWO | Shrub/scrub | 0.2 | 40.0543 | -105.5820 | 2015 to 2018 |
| Onaqui | ONAQ | Shrub/scrub | 1.2 | 40.1776 | -112.4520 | 2014 to 2018 |
| Oak Ridge | ORNL | Deciduous broadleaf | 28.0 | 35.9641 | -84.2826 | 2015 to 2018 |
| Ordway-Swisher Biological Station | OSBS | Evergreen needleleaf | 23.0 | 29.6893 | -81.9934 | 2013 to 2018 |
| Smithsonian Conservation Biology Institute | SCBI | Deciduous broadleaf | 35.0 | 38.8929 | -78.1395 | 2015 to 2018 |
| Smithsonian Environmental Research Center | SERC | Deciduous broadleaf | 38.0 | 38.8901 | -76.5600 | 2015 to 2018 |
| Steigerwaldt Land Services | STEI | Mixed forest | 5.5 | 45.5089 | -89.5864 | 2016 to 2018 |
| North Sterling | STER | Cultivated crops | 1.0 | 40.4619 | -103.0290 | 2014 to 2018 |
| Talladega National Forest | TALL | Deciduous broadleaf | 25.0 | 32.9505 | -87.3933 | 2015 to 2018 |
| UNDERC | UNDE | Woody wetlands | 24.0 | 46.2339 | -89.5373 | 2015 to 2018 |
| Woodworth | WOOD | Grassland/herbaceous | 1.0 | 47.1282 | -99.2414 | 2014 to 2018 |

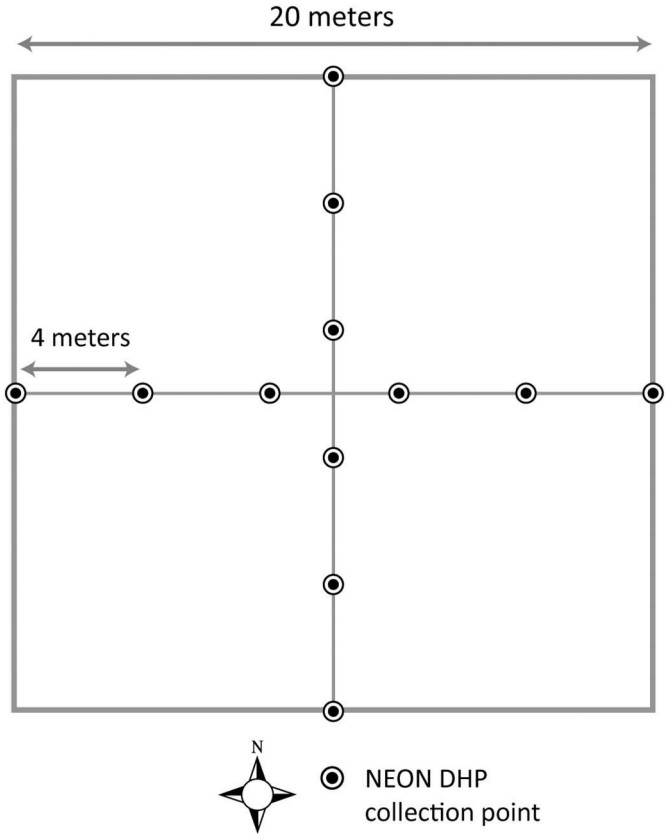


**Fig. 3.** Within each NEON plot, DHP images are acquired at twelve points arranged in a cross pattern.

resolution imagery was utilised. The most widely used upscaling method involves the derivation of an empirical transfer function relating the in situ reference measurements to the radiometric information in the high spatial resolution imagery (Baret et al., 2005; Camacho et al., 2013; Fang et al., 2012; Fernandes et al., 2014; Garrigues et al., 2008a; Martínez et al., 2009; Morisette et al., 2006; Yan et al., 2016b). To successfully implement this method, a minimum of twenty ESUs are typically recommended (Morisette et al., 2006). Because NEON routinely sample only three ESUs on a given date at each site, a robust transfer function could not be derived for each individual high spatial resolution image. As a result, in previous releases of the GBOV dataset (V1 and V2), a multitemporal approach was instead adopted, in which transfer functions relating vegetation indices and in situ reference measurements were established using data from all acquisition dates, following the approach of Campos-Taberner et al. (2016) and Yin et al. (2017).

Despite the potential of multitemporal transfer functions (Campos-Taberner et al., 2016; Yin et al., 2017), the limited spatial sampling at NEON sites necessarily reduces the extent to which variability can be captured at the site scale, and since release, analysis of the GBOV transfer functions has revealed several shortcomings. These include weak predictive power over some sites, limited extrapolation capabilities when transfer functions are applied to images acquired outside of the time period represented in their training data, and, in several cases, poorly resolved vegetation seasonality (Sánchez-Zapero et al., 2018). To overcome the limitations of the existing upscaling approach, in this paper we developed a new RTM-based upscaling framework, making use of the Sentinel-2 Level 2 Prototype Processor (SL2P) developed by Weiss and Baret (2016). In such an approach, the in situ reference measurements are used to a) evaluate the performance of the RTM-based retrievals, and b) facilitate calibration, to correct for any observed biases (Baret et al., 2005; Fang et al., 2019b; Fernandes et al., 2014; Tan et al., 2005; Yang et al., 2006; Tian et al., 2002; Xu et al., 2018). Importantly, a major advantage of the RTM-based approach is reduced sensitivity to the spatial representativeness of the in situ reference measurements themselves (Baret et al., 2005).

SL2P is a hybrid retrieval algorithm that makes use of artificial neural networks (ANNs) trained using the Leaf Optical Properties Spectra (PROSPECT) and Scattering by Arbitrarily Inclined Leaves (SAIL) RTMs (Feret et al., 2008; Verhoef et al., 2007). In addition to LAI and FAPAR, SL2P enables estimation of the fraction of vegetation cover (FCOVER), canopy chlorophyll content (CCC), and canopy water content (CWC) from MSI bottom-of-atmosphere reflectance data. Evaluation efforts have demonstrated good performance over crop canopies, but underestimation of higher LAI values such as those observed over forests (Brown et al., 2019b; Djamai et al., 2019; Pasqualotto et al., 2019; Vanino et al., 2018; Vuolo et al., 2012; Xie et al., 2019). These results are to be expected given the one-dimensional nature of the SAIL RTM; crop canopies better conform its turbid medium assumption, whereas forests are characterised by increased heterogeneity, foliage clumping, and shadowing (factors not accounted for by SAIL) (Richter et al., 2009; Verger et al., 2011).

The shortcomings of SL2P over forest environments highlight the importance of calibrating retrievals with in situ reference measurements. Provided that retrievals are consistently biased, and assuming that the in situ reference measurements adequately account for factors such as foliage clumping, a calibration function can be used to correct for these biases. Such an approach has successfully been applied to correct for the underestimation of higher LAI values by other hybrid retrieval algorithms trained using PROSPECT and SAIL (Duveiller et al., 2011). It is worth noting that because aggregation of the high spatial resolution reference maps acts to substantially reduce random errors (Brown et al., 2019; Camacho et al., 2013; Canisius et al., 2010; Fernandes et al., 2014; Garrigues et al., 2008a), addressing random errors is much less of a concern than correcting for biases.

Before executing SL2P, we derived L2A bottom-of-atmosphere reflectance from all L1C MSI scenes available during the study period, using Sen2Cor 2.5.5 to perform the atmospheric correction (Müller-Wilm, 2018). Once LAI and FAPAR were estimated, calibration functions were derived through ordinary least squares (OLS) regression analysis (Brown et al., 2019), making use of in situ reference measurements acquired within one day of each MSI scene. The use of OLS enabled both additive and multiplicative biases to be corrected for. To ensure a consistent area of analysis when deriving the calibration functions, a footprint matching procedure was adopted. In situ values were compared with the mean of a variable window of MSI pixels, whose size was determined according to the ESU measurement footprint at each site. Assuming DHP images were acquired at a shoulder height of 1.5 m above the ground (Meier et al., 2018), and using the mean canopy heights listed in Table 2, ESU measurement footprints were calculated as

$$2\,h\tan\theta + l$$

where $h$ is the distance between the camera and the top of the canopy (or the ground in the case of sites with only downwards-facing images), $\theta$ is the maximum zenith angle of the measurement, and $l$ is the one-sided length of the ESU. At each site, the smallest odd window size containing the entire ESU measurement footprint was selected.

### 3.6. Quality control and spatiotemporal matchup procedure

Analysis of the considered LAI and FAPAR products was carried out over a 1.5 km x 1.5 km area centred on the location of each site's tower (3 x 3 pixels for the MOD152AH/VNP15A2H products and 5 x 5 pixels for the CGLS 300 m V1 products). This extent was selected in order to a) reduce the impact of positional uncertainties and those related to instrument characteristics such as the point spread function (PSF), and b) provide a common spatial support for all considered products. For each

product, the mean of all valid pixels was computed over the 1.5 km x 1.5 km area, provided that greater than 50% of pixels were valid (Camacho et al., 2013; Garrigues et al., 2008a). In the case of the MOD15A2H and VNP15A2H products, only good quality retrievals produced using the main algorithm were considered.

Product evaluation was achieved by comparing the LAI and FAPAR products with the high spatial resolution reference maps described in Section 3.5. Again, the mean of all valid pixels in the high spatial resolution reference map was computed over a 1.5 km x 1.5 km area, provided greater than 50% of pixels were valid (invalid pixels included pixels classified by Sen2Cor as saturated/defective, dark, cloud/cloud shadow, water, thin cirrus, or snow, in addition to unclassified pixels, and retrievals flagged by SL2P as having an out of range input/output). For all considered LAI and FAPAR products, each high spatial resolution reference map was matched to the compositing period within which it fell, whilst the maximum value was selected if more than one high spatial resolution reference map was available within a given compositing period.

Finally, intercomparison was carried out to assess the consistency of the LAI and FAPAR products. Because the MOD15A2H and VNP15A2H products share the same eight-day temporal compositing scheme, they could be compared directly. To facilitate comparison with the ten-day CGLS 300 m V1 products, corresponding MOD15A2H and VNP15A2H products were selected if their nominal dates fell within the considered compositing period. If more than one product fell within the compositing period, the maximum value was selected, providing an additional means of quality control (Holben, 1986).

### 3.7. Evaluation metrics

Overall agreement was assessed using the coefficient of determination ($r^2$) and root mean square difference (RMSD). To enable comparison between products of different units, a normalised RMSD (NRMSD) was calculated by dividing the RMSD by the mean of the reference values (Richter et al., 2012). Bias was determined as the mean difference. For evaluation against high spatial resolution reference maps, the uncertainty agreement ratio (UAR) was also calculated, corresponding to the percentage of retrievals falling within 1 unit or 20% for LAI, and 0.1 unit or 20% for FAPAR. For LAI, these correspond to the uncertainty requirements defined within the Sentinels for Science project (SEN4SCI, 2011). It is worth noting that stricter requirements (15% for LAI and 0.05 unit or 10% for FAPAR) are defined by GCOS (2019). However, because uncertainties associated with the in situ reference measurements themselves (1 unit for LAI and 0.1 unit for FAPAR) typically exceed these requirements (Camacho et al., 2013; Garrigues et al., 2008a), compliance with them cannot reliably be assessed. To better understand the performance of the products over different environments, phenological phases, and time periods, statistics were also calculated per land cover type, meteorological season, and year.

## 4. Results

### 4.1. Consistency of PAI and FIPAR derived from DHP data

When the DHP-derived in situ reference measurements were compared, a strong relationship between PAI and FIPAR was observed ($r^2$ = 0.98), resembling the known association between these variables under the assumption of a turbid medium, which is characterised by asymptotic saturation (Fig. 4). Scatter around this relationship was minimal, and outliers were primarily restricted to individual in situ reference measurements over deciduous broadleaf forest, evergreen needleleaf forest and pasture/hay sites (Fig. 4).

### 4.2. Impact of neglecting the understory layer in forest environments

When derived using only upwards-facing DHP images representing the overstory layer, total PAI and FIPAR were underestimated at forest sites (Fig. 5). A mean underestimation of 0.54 was observed in the case of PAI, although in the worst case, an underestimation of 3.48 occurred. Greater underestimation was observed at higher PAI values. The overall difference in PAI when neglecting the understory, as quantified by the RMSD (NRMSD), was 0.76 (21%) (Fig. 5a). In terms of FIPAR, the mean underestimation was 0.07, whilst in the worst case, an underestimation of 0.61 was observed. The RMSD (NRMSD) in FIPAR when neglecting the understory layer was 0.11 (14%) (Fig. 5b).

### 4.3. Accuracy of high spatial resolution reference maps

The high spatial resolution reference maps demonstrated good agreement with in situ reference measurements of both PAI ($r^2$ = 0.87, RMSD = 0.78, NRMSD = 29%) and FIPAR ($r^2$ = 0.88, RMSD = 0.13, NRMSD = 21%). For FIPAR, slight overestimation was observed over deciduous broadleaf forest, whilst underestimation occurred over some grassland/herbaceous and pasture/hay ESUs. Nevertheless, for both variables, the majority of values fell within the uncertainty requirements described in Section 3.7 (84% for PAI and 76% for FIPAR) (Fig. 6). The accuracy of the high spatial resolution reference maps was comparable to those used in previous EO product evaluation exercises (Canisius et al., 2010; De Kauwe et al., 2011; Fang et al., 2019a, 2019b; Heiskanen et al., 2012; Xu et al., 2018; Yin et al., 2017), confirming their suitability to act as a reference dataset for product evaluation.

### 4.4. Evaluation of products against high spatial resolution reference maps

Of the considered products, the CGLS 300 m V1 product demonstrated the best overall agreement with the high spatial resolution reference maps, exhibiting the strongest relationships and lowest RMSD values in the case of both LAI ($r^2$ = 0.92, RMSD = 0.57, NRMSD = 24%) and FAPAR ($r^2$ = 0.93, RMSD = 0.08, NRMSD = 14%) (Fig. 7a). Overall, 92% of LAI and 89% of FAPAR retrievals met the uncertainty requirements. These results were confirmed by qualitative evaluation of the product time series, which better matched reference PAI values over the majority of sites when compared to the MOD15A2H/VNP15A2H products (Fig. 8). Nevertheless, reasonable agreement with reference data was also achieved by the MOD15A2H and VNP15A2H products, with 80% and 83% of LAI retrievals and 69% and 66% of FAPAR retrievals meeting the uncertainty requirements, respectively. For LAI, slightly better agreement was demonstrated by the VNP15A2H product ($r^2$ = 0.76, RMSD = 0.81, NRMSD = 36%) than the MOD15A2H product ($r^2$ = 0.74, RMSD = 0.89, NRMSD = 39%), whilst agreement was similar in terms of FAPAR ($r^2$ = 0.84 to 0.85, RMSD = 0.12, NRMSD = 20% to 21%) (Fig. 7).

When analysed by land cover type, the CGLS 300 m V1 product exhibited the best agreement with the high spatial resolution reference maps in all cases for FAPAR, and in all cases except grassland/herbaceous vegetation and mixed forest for LAI (where the best agreement was with the VNP15A2H and MOD15A2H products) (Table 3). Over sparse canopies such as shrub/scrub vegetation, all products demonstrated an apparent overestimation of FAPAR when compared to reference FIPAR values (Fig. 7), reflected by positive biases (Table 3). This was most pronounced in the MOD15A2H and VNP15A2H products, whilst biases were slightly reduced in the CGLS 300 m V1 product (Fig. 7). Such overestimation was not observed for LAI. When compared to reference PAI and FIPAR values, the MOD15A2H and VNP15A2H products substantially underestimated LAI and FAPAR over pasture/hay (Fig. 7), reflected by negative biases of between -1.56 and -1.58 for LAI, and -0.14, and -0.16 for FAPAR (Table 3). Biases over all other land cover types were within 1 unit for LAI, and 0.1 unit for FAPAR (i.e. the typical uncertainty associated with in situ reference

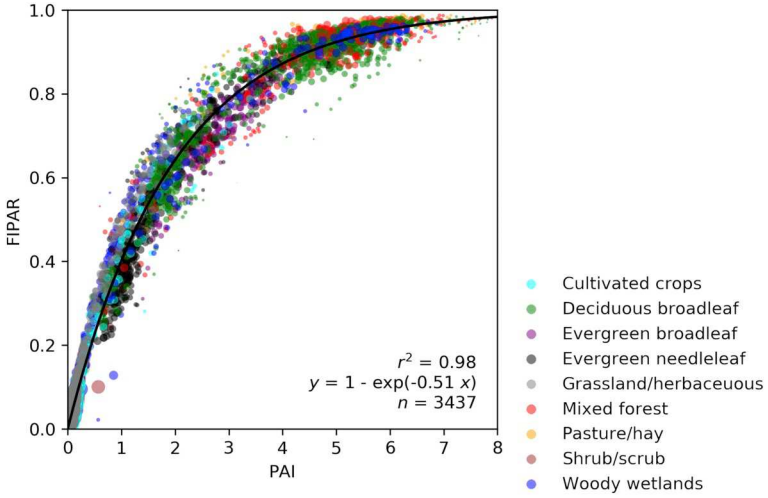


**Fig. 4.** Comparison between DHP-derived PAI and FIPAR. Points are scaled by their density.

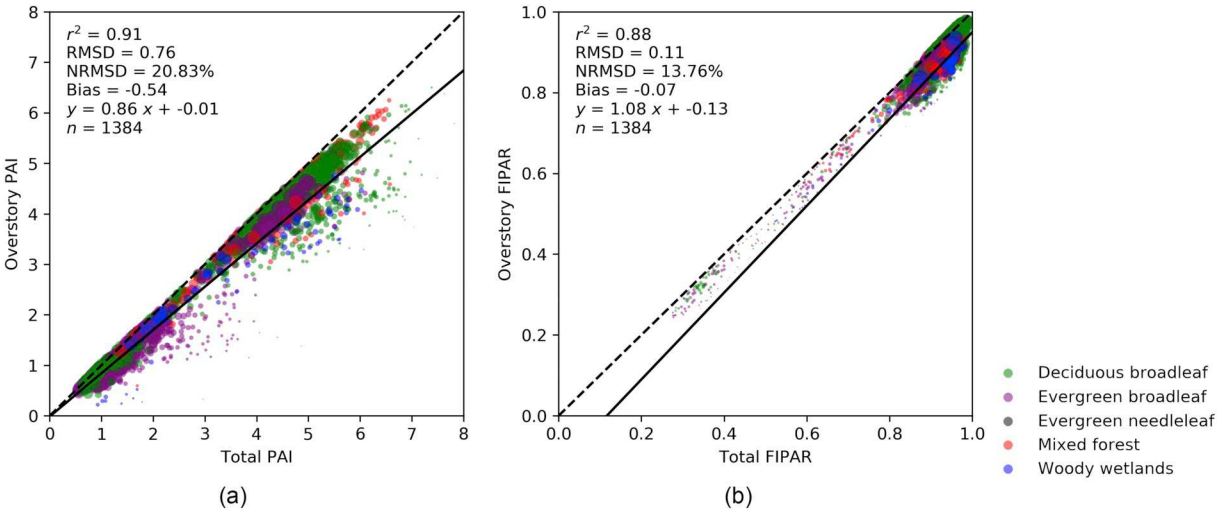


**Fig. 5.** Relationship between in situ reference measurements of total and overstory PAI (a) and FIPAR (b) at forest sites. Points are scaled by their density.

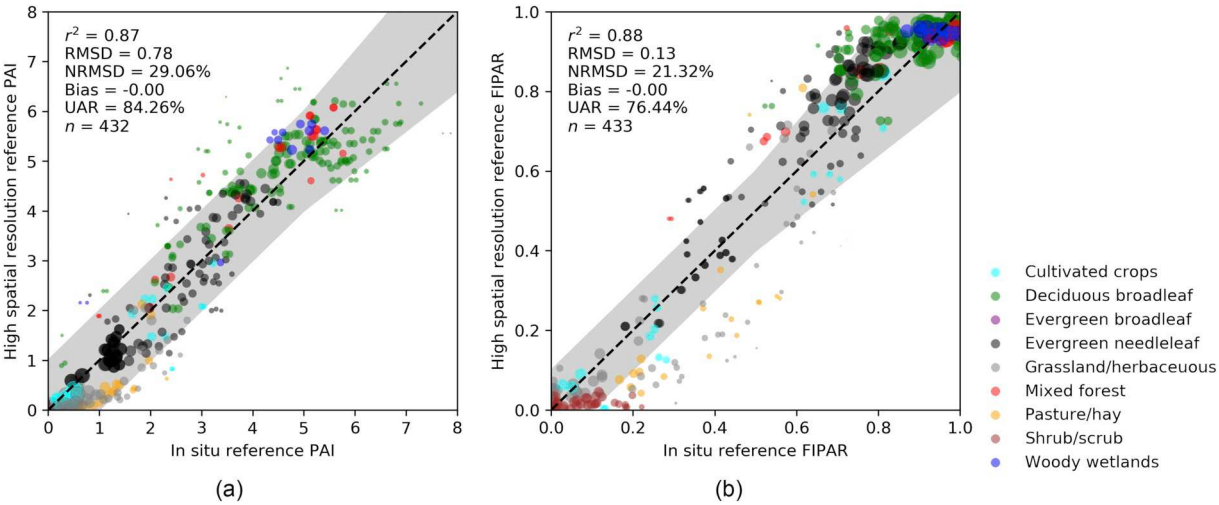


**Fig. 6.** Comparison between high spatial resolution reference maps and in situ reference measurements of PAI (a) FIPAR (b). The dashed line represents a 1:1 relationship, whilst the shaded grey area represents the uncertainty requirements. Note that a different number of points were available for PAI and FIPAR due to differences in the availability of valid data. Points are scaled by their density.

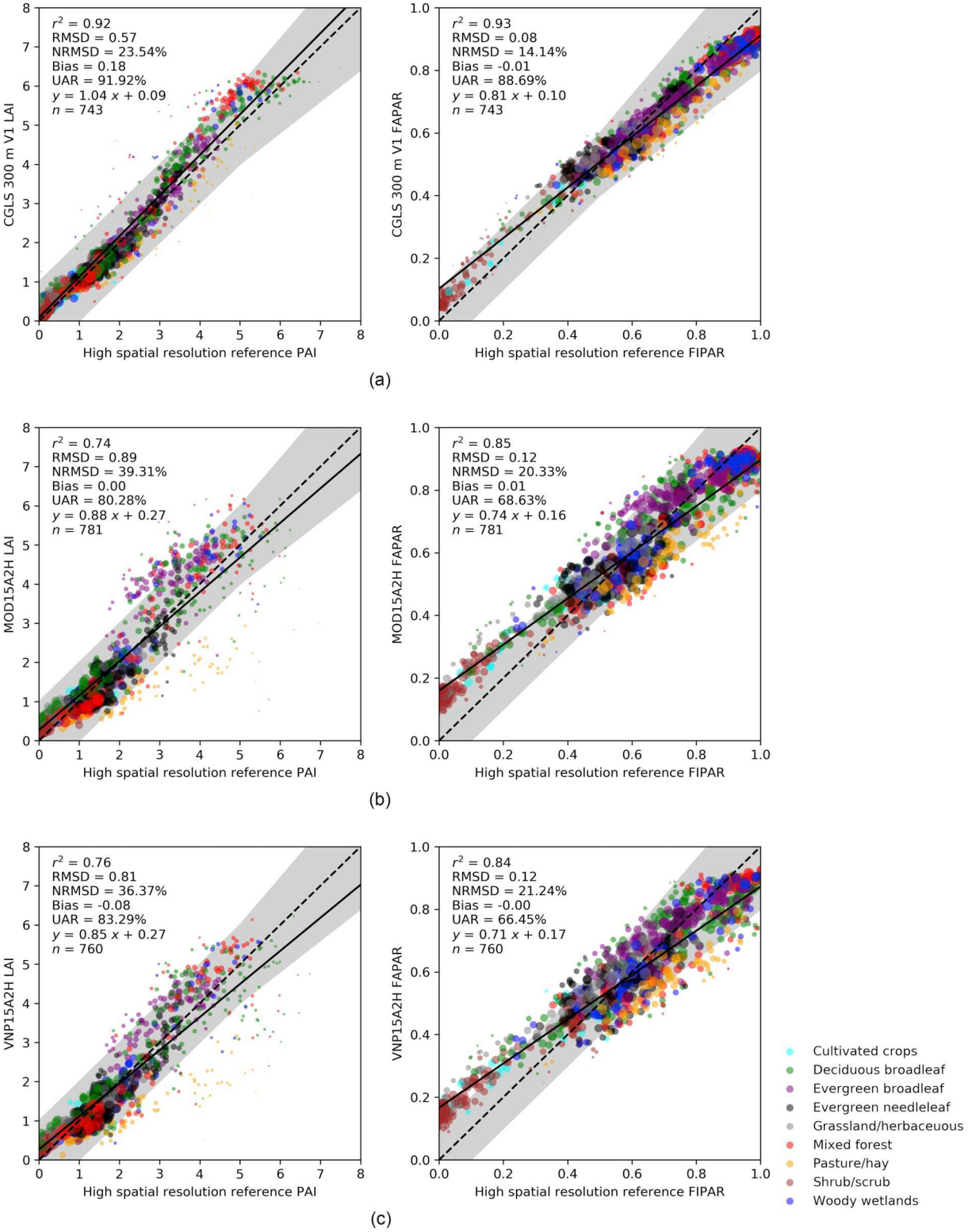


**Fig. 7.** Evaluation of CGLS 300 m V1 (a), MOD15A2H (b) and VNP15A2H (c) LAI (left) and FAPAR (right) products against high spatial resolution reference maps. The dashed line represents a 1:1 relationship, whilst the shaded grey area represents the uncertainty requirements. Note that a different number of points were available for each product due to differences in temporal resolution, the time period covered, and availability of valid data. Points are scaled by their density.

measurements).

When analysed by meteorological season, all products demonstrated the best agreement with the high spatial resolution reference maps during the winter. This was true for both LAI ($r^2$ = 0.87 to 0.95, RMSD = 0.31 to 0.55, NRMSD = 24% to 41%) and FAPAR ($r^2$ = 0.91 to 0.96, RMSD = 0.07 to 0.10, NRMSD = 16% to 22%) (Appendix C). For the CGLS 300 m V1 product, the worst agreement occurred during the spring ($r^2$ = 0.85, RMSD = 0.68, NRMSD = 33% for LAI and $r^2$ = 0.89, RMSD = 0.10, NRMSD = 19% for FAPAR). Nevertheless, 87% of LAI and 76% of FAPAR retrievals still met the uncertainty

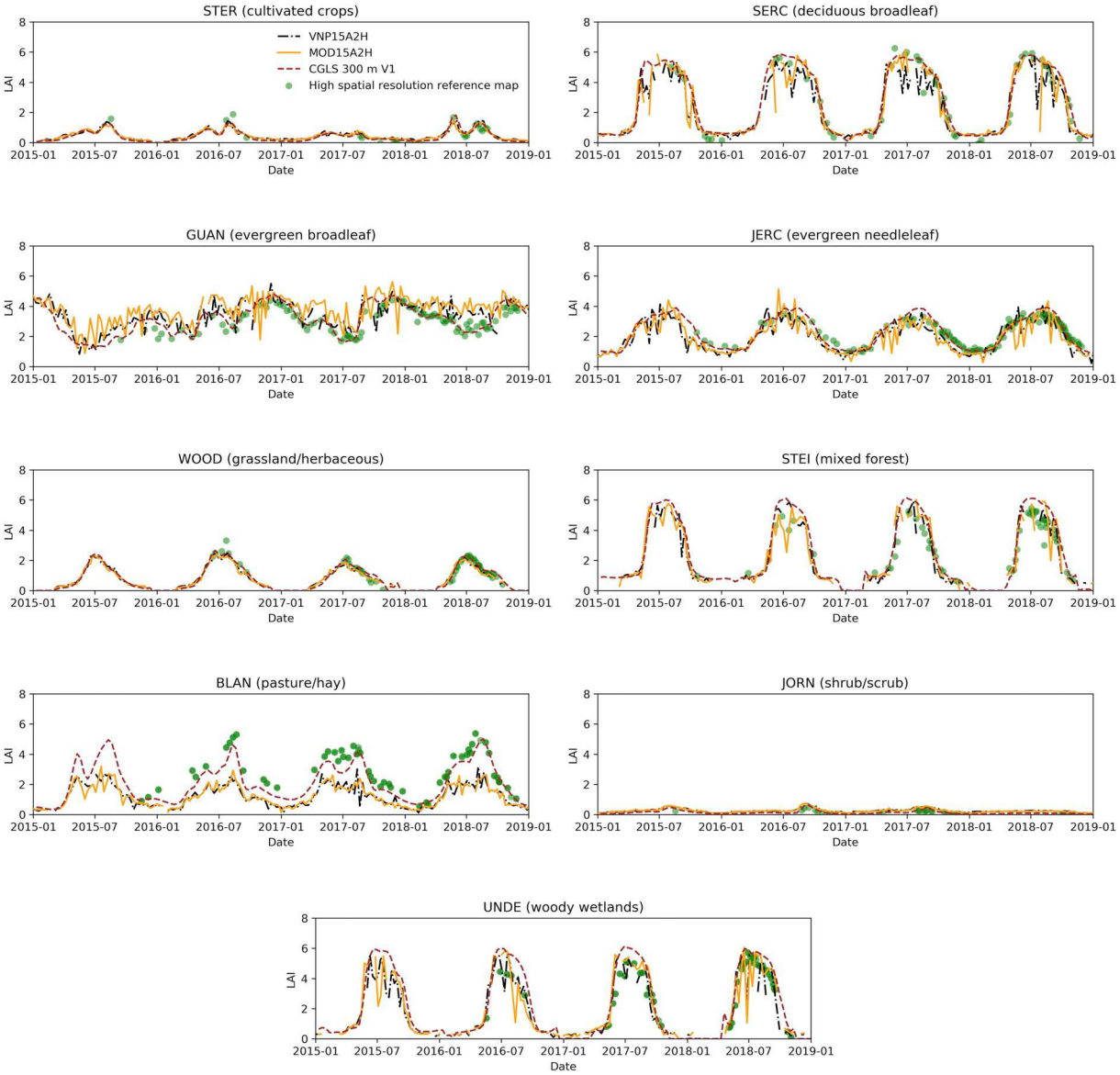


**Fig. 8.** Example time series of CGLS 300 m V1, MOD15A2H and VNP15A2H LAI products over sites of each land cover type, in addition to high spatial resolution reference PAI (refer to Table 2 for site codes).

requirements. In contrast, the worst agreement occurred during the summer for the MOD15A2H and VNP15A2H products ($r^2$ = 0.59 to 0.66, RMSD = 1.08 to 1.21, NRMSD = 35% to 39% for LAI and $r^2$ = 0.76 to 0.79, RMSD = 0.14, NRMSD = 21% for FAPAR), where 69% to 75% of LAI and 64% to 68% of FAPAR retrievals met the uncertainty requirements. In terms of annual variations in agreement, for all products, differences between years were small, with the exception of 2015 (whose results should be considered less reliable due to the limited number of valid data points available) (Appendix C).

### 4.5. Intercomparison of products

Overall, the best agreement between the considered products was demonstrated by the MOD15A2H and VNP15A2H products, which exhibited the strongest relationships, lowest RMSD values, and minimal biases in the case of both LAI ($r^2$ = 0.89, RMSD = 0.50, NRMSD = 33%) and FAPAR ($r^2$ = 0.92, RMSD = 0.07, NRMSD = 15%) (Fig. 9c). Agreement between the CGLS 300 m V1 product and the MOD15A2H/VNP15A2H products was also good, although slightly better in the case of the VNP15A2H product (Fig. 9). Notably, when compared to the MOD15A2H/VNP15A2H products, the CGLS 300 m V1 product was characterised by an underestimation of FAPAR over sparse canopies such as shrub/scrub vegetation, reflecting the negative biases associated with these sites (Table 4), whilst such underestimation was not so evident for LAI (Fig. 9). An underestimation of LAI and FAPAR was also observed over evergreen broadleaf forest (Fig. 9), whilst an overestimation of LAI was apparent over deciduous forest and pasture/hay, again reflecting the biases observed for these land cover types (Table 4).

In terms of their temporal characteristics, whilst the MOD15A2H and VNP15A2H products demonstrated the best temporal consistency, they were characterised by a greater degree of high frequency noise than the CGLS 300 m V1 product, which exhibited considerably smoother temporal sequences overall (Fig. 8). This was most pronounced over evergreen broadleaf forest, where seasonal patterns were poorly resolved by the MOD15A2H and VNP15A2H products. In contrast, the CGLS 300 m V1 product demonstrated more plausible temporal sequences, capturing peaks and troughs in LAI in a convincing manner whilst varying smoothly over time. The MOD15A2H and VNP15A2H products tracked seasonal patterns in a more realistic way over deciduous broadleaf forest, evergreen needleleaf forest, pasture/

**Table 3**
Evaluation against high spatial resolution reference maps, by land cover type. Note that a different number of points were available for each product due to differences in temporal resolution, the time period covered, and availability of valid data. The products with the lowest RMSD for each land cover type are shown in bold.

| | | CGLS 300 m V1 | | | | | MOD15A2H | | | | | VNP15A2H | | | | | |
|---|---|---|---|---|---|---|---|---|---|---|---|---|---|---|---|---|---|
| | Land cover | $r^2$ | RMSD | NRMSD (%) | Bias | UAR (%) | *n* | $r^2$ | RMSD | NRMSD (%) | Bias | UAR (%) | *n* | $r^2$ | RMSD | NRMSD (%) | Bias | UAR (%) | *n* |
| LAI | Cultivated crops | **0.81** | **0.28** | **37.84** | **-0.02** | **94.44** | **17** | 0.82 | 0.35 | 54.43 | 0.08 | 100.00 | 20 | 0.72 | 0.39 | 60.26 | 0.12 | 100.00 | 20 |
| | Deciduous broadleaf | **0.93** | **0.63** | **19.06** | **0.32** | **90.80** | **174** | 0.70 | 1.05 | 34.38 | 0.02 | 79.14 | 163 | 0.77 | 0.90 | 29.67 | -0.05 | 79.11 | 158 |
| | Evergreen broadleaf | **0.77** | **0.47** | **15.11** | **0.20** | **96.25** | **80** | 0.39 | 1.11 | 35.51 | 0.90 | 52.38 | 84 | 0.54 | 0.77 | 24.49 | 0.54 | 75.31 | 81 |
| | Evergreen needleleaf | **0.93** | **0.25** | **13.01** | **0.00** | **100.00** | **111** | 0.73 | 0.48 | 24.54 | -0.20 | 97.60 | 125 | 0.78 | 0.42 | 21.50 | -0.14 | 98.36 | 122 |
| | Grassland/herbaceous | 0.91 | 0.33 | 30.27 | 0.14 | 100.00 | 42 | 0.92 | 0.34 | 28.30 | 0.01 | 98.08 | 52 | **0.94** | **0.32** | **26.89** | **0.02** | **100.00** | **51** |
| | Mixed forest | 0.89 | 0.91 | 26.06 | 0.52 | 73.40 | 94 | **0.81** | **0.86** | **27.26** | **0.08** | **72.22** | **90** | 0.76 | 0.93 | 29.51 | -0.08 | 75.58 | 86 |
| | Pasture/hay | **0.89** | **0.69** | **22.23** | **-0.53** | **89.80** | **49** | 0.77 | 1.76 | 58.30 | -1.56 | 24.53 | 53 | 0.70 | 1.79 | 59.20 | -1.58 | 24.53 | 53 |
| | Shrub/scrub | **0.94** | **0.19** | **75.22** | **0.15** | **100.00** | **97** | 0.89 | 0.27 | 107.59 | 0.14 | 100.00 | 109 | 0.85 | 0.29 | 117.99 | 0.15 | 100.00 | 108 |
| | Woody wetlands | **0.89** | **0.68** | **27.87** | **0.22** | **86.08** | **79** | 0.76 | 0.80 | 32.26 | 0.06 | 87.06 | 85 | 0.76 | 0.72 | 29.83 | -0.10 | 86.42 | 81 |
| FAPAR | Cultivated crops | **0.84** | **0.06** | **22.44** | **0.00** | **83.33** | **17** | 0.85 | 0.10 | 38.98 | 0.07 | 50.00 | 20 | 0.75 | 0.12 | 44.85 | 0.08 | 45.00 | 20 |
| | Deciduous broadleaf | **0.90** | **0.09** | **12.36** | **-0.02** | **88.51** | **174** | 0.70 | 0.14 | 19.23 | 0.00 | 75.46 | 163 | 0.76 | 0.12 | 17.60 | -0.01 | 73.42 | 158 |
| | Evergreen broadleaf | **0.82** | **0.07** | **9.32** | **-0.02** | **95.00** | **80** | 0.66 | 0.10 | 13.90 | 0.04 | 73.81 | 84 | 0.55 | 0.10 | 13.40 | 0.00 | 85.19 | 81 |
| | Evergreen needleleaf | **0.81** | **0.05** | **9.54** | **0.00** | **94.59** | **111** | 0.46 | 0.09 | 15.91 | -0.01 | 80.80 | 125 | 0.51 | 0.09 | 15.19 | 0.00 | 78.69 | 122 |
| | Grassland/herbaceous | **0.91** | **0.10** | **28.17** | **0.07** | **64.29** | **42** | 0.88 | 0.12 | 31.25 | 0.08 | 63.46 | 52 | 0.94 | 0.12 | 30.26 | 0.09 | 60.78 | 51 |
| | Mixed forest | **0.79** | **0.10** | **13.04** | **-0.05** | **84.04** | **94** | 0.74 | 0.11 | 14.30 | -0.05 | 80.00 | 90 | 0.64 | 0.13 | 17.38 | -0.06 | 74.42 | 86 |
| | Pasture/hay | **0.89** | **0.12** | **16.41** | **-0.11** | **83.67** | **49** | 0.81 | 0.16 | 22.06 | -0.14 | 50.94 | 53 | 0.63 | 0.19 | 26.34 | -0.16 | 43.40 | 53 |
| | Shrub/scrub | **0.96** | **0.06** | **53.89** | **0.05** | **93.81** | **97** | 0.88 | 0.12 | 99.89 | 0.10 | 32.11 | 109 | 0.84 | 0.12 | 108.34 | 0.10 | 27.78 | 108 |
| | Woody wetlands | **0.84** | **0.08** | **12.72** | **-0.01** | **89.87** | **79** | 0.74 | 0.10 | 15.57 | 0.00 | 85.88 | 85 | 0.71 | 0.11 | 16.81 | -0.02 | 82.72 | 81 |

hay, and woody wetlands, but were still subject to noisier time-series than the CGLS 300 m V1 product. Over cultivated crops, grassland/herbaceous, and shrub/scrub vegetation, all products demonstrated comparable temporal sequences, and the MOD15A2H and VNP15A2H products were subject to considerably less high frequency noise than over the other considered land cover types (Fig. 8).

## 5. Discussion

### 5.1. Consistency of products and agreement with reference data

Whilst the very good agreement observed during intercomparison of the MOD15A2H and VNP15A2H products is to be expected due to the similar instruments and retrieval schemes they adopt, the low bias observed provides confidence in the ability of the VNP15A2H product to provide continuity to the MOD15A2H product. This is an important consideration, as the MODIS instruments are reaching the end of their operational lives and are expected to be retired within the coming years (Yan et al., 2018). The good agreement between the CGLS 300 m V1 and MOD15A2H/VNP15A2H products is likely because the CGLS 300 m V1 product is trained, in part, using the Collection 5 MOD15A2 product, and reflects the result of previous studies that have compared Collection 5 MOD15A2 and GEOV1 retrievals (Camacho et al., 2013; Fang et al., 2013; Weiss et al., 2014). The CGLS 300 m V1 product's underestimation of lower FAPAR values when compared to the MOD15A2H/VNP15A2H products is a direct consequence of the dataset used to train the underlying ANN, which was specifically developed to address overestimation by the MOD15 retrieval scheme.

In terms of evaluation against reference data, the results of this study confirm those of previous exercises, albeit with a substantially increased number of samples. The superior agreement with reference data achieved by the CGLS 300 m V1 product reflects the results of Camacho et al. (2013) and Weiss et al. (2014), who reported that the related GEOV1 product, which shares a similar retrieval scheme, outperforms a variety of other LAI and FAPAR products. The increased accuracy of GEOV1 retrievals when compared to the Collection 5 MOD15A2 product has been reported in several global evaluation exercises (Camacho et al., 2013; Tao et al., 2015; Weiss et al., 2014; Xu et al., 2018). For the GEOV1 product, these studies reported RMSD values of 0.74 to 0.82 for LAI, and 0.08 to 0.12 for FAPAR. Our analyses indicate that the CGLS 300 m V1 product yields similar or improved results (RMSD = 0.57 for LAI and 0.08 for FAPAR), whilst providing data at a spatial resolution much closer to the 250 m required by GCOS (2019) (i.e. 300 m as opposed to 1 km).

It is worth noting that our results indicate the CGLS 300 m V1 product provides considerably better performance than recently found by Fuster et al. (2020), who reported an RMSD of 1.08 for LAI and 0.11 for FAPAR. However, their study was restricted to cultivated crops, which were less well represented in our study than the other considered land cover types. When compared with the MOD15A2H FAPAR retrievals, the reduced biases observed over shrub/scrub sites in the case of the CGLS 300 m V1 product highlight the value of its retrieval approach. As also noted by Fuster et al. (2020), the performance of the CGLS 300 m V1 product is further demonstrated by the smoother (and more realistic) temporal sequences demonstrated in the product time series when compared to the nosier MOD15A2H/VNP15A2H products, which make use of a less sophisticated temporal compositing scheme.

With respect to the MOD15A2H product, our evaluation results (RMSD = 0.89 for LAI and 0.12 for FAPAR) are comparable to those of Yan et al., 2016b, who reported an RMSD of 0.66 for LAI and 0.15 for FAPAR. The apparent overestimation of lower FAPAR values observed in this study was also reported by Yan et al., 2016b, who too noted overestimation of FAPAR over sparsely vegetated areas when compared to upscaled in situ data. Similar results were presented by Weiss et al. (2014) and Tao et al. (2015) when evaluating the GEOV1 and Collection 5 MOD15A2 products, and by Fensholt et al. (2004) when assessing

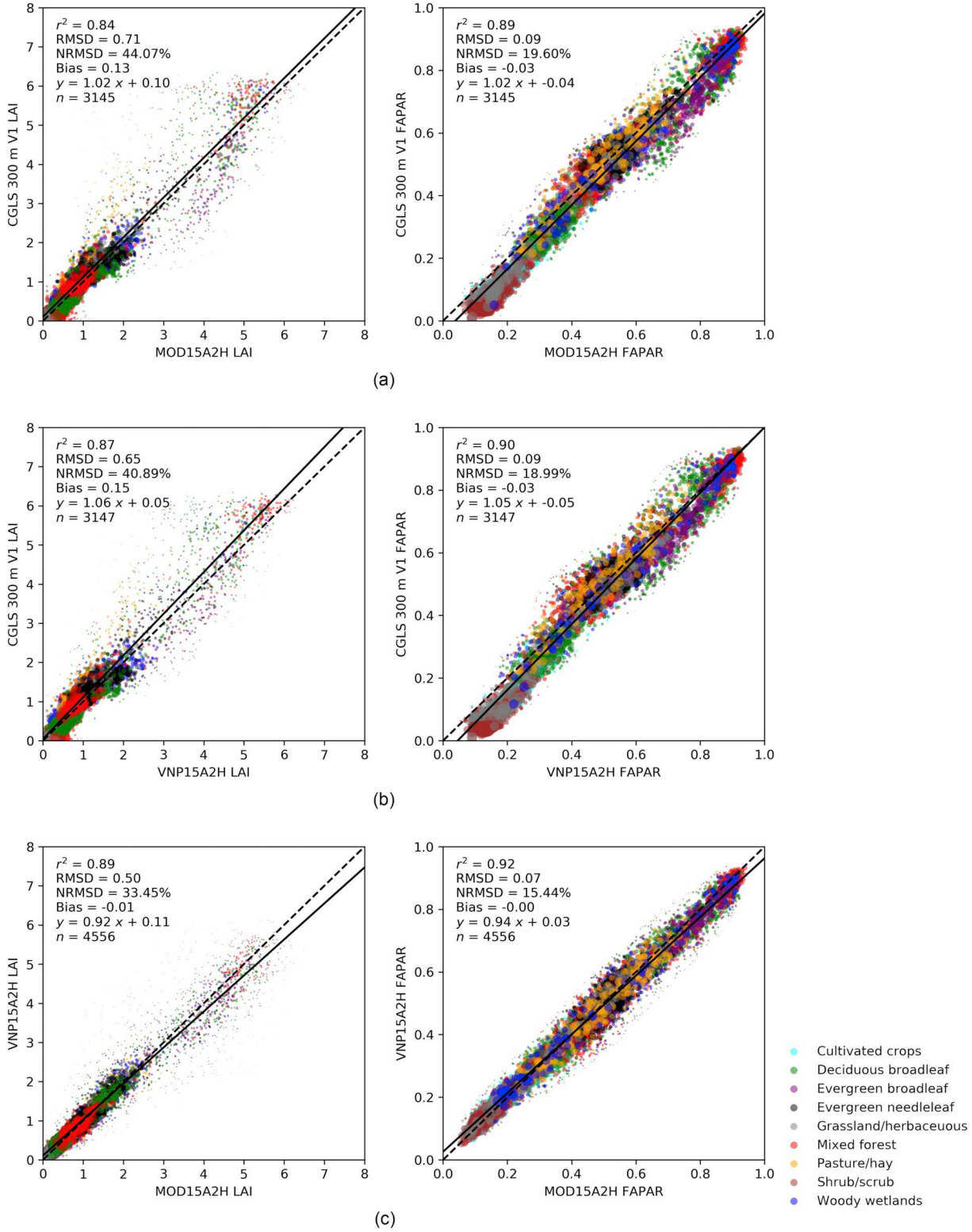


**Fig. 9.** Intercomparison of CGLS 300 m V1 and MOD15A2H (a), CGLS 300 m V1 and VNP15A2H (b), and MOD15A2H and VNP15A2H (c) LAI (left) and FAPAR (right) products. The dashed line represents a 1:1 relationship. Note that a different number of points were available for each product due to differences in temporal resolution, the time period covered, and availability of valid data. Points are scaled by their density

Collection 4 MOD15A2 retrievals. Indeed, our analysis reveals the issue to be prevalent over shrub/scrub sites, at which less dense vegetation canopies might be expected than in forest environments. Yan et al., 2016b suggested that the apparent overestimation may be due to a lack of understory characterisation in their in situ reference measurements. The fact that the same result is observed in our study, in which understories were considered, suggests this is unlikely to be the case.

A further explanation for the apparent biases observed in this study is related to the differing assumptions of the in situ reference measurements and the considered products, which cause them to be

**Table 4**
Intercomparison of products, by land cover type. Note that a different number of points were available for each product due to differences in temporal resolution, the time period covered, and availability of valid data. The products with the lowest RMSD for each land cover type are shown in bold.

| | | CGLS 300 m V1 vs MOD15A2H | | | | | CGLS 300 m V1 vs VNP15A2H | | | | | MOD15A2H vs VNP15A2H | | | | |
|---|---|---|---|---|---|---|---|---|---|---|---|---|---|---|---|---|
| | Land cover | $r^2$ | RMSD | NRMSD (%) | Bias | $n$ | $r^2$ | RMSD | NRMSD (%) | Bias | $n$ | $r^2$ | RMSD | NRMSD (%) | Bias | $n$ |
| LAI | Cultivated crops | 0.92 | 0.13 | 26.65 | -0.05 | 172 | 0.92 | 0.13 | 25.83 | -0.07 | 172 | **0.90** | **0.10** | **22.00** | **0.02** | **260** |
| | Deciduous broadleaf | 0.78 | 1.01 | 42.76 | 0.28 | 637 | 0.82 | 0.95 | 41.31 | 0.31 | 641 | **0.87** | **0.63** | **29.48** | **-0.03** | **877** |
| | Evergreen broadleaf | 0.53 | 1.05 | 26.81 | -0.78 | 178 | 0.52 | 0.83 | 23.52 | -0.42 | 175 | **0.38** | **0.80** | **21.20** | **-0.26** | **264** |
| | Evergreen needleleaf | 0.74 | 0.45 | 26.22 | 0.14 | 357 | **0.76** | **0.42** | **24.24** | **0.10** | **358** | 0.67 | 0.46 | 28.15 | 0.05 | 542 |
| | Grassland/herbaceous | 0.97 | 0.14 | 22.17 | 0.01 | 300 | 0.96 | 0.14 | 22.04 | 0.00 | 299 | **0.96** | **0.11** | **18.17** | **0.01** | **445** |
| | Mixed forest | 0.87 | 0.85 | 36.02 | 0.32 | 430 | **0.91** | **0.72** | **30.32** | **0.32** | **435** | 0.85 | 0.75 | 33.50 | -0.01 | 589 |
| | Pasture/hay | 0.84 | 1.11 | 91.18 | 0.87 | 174 | 0.87 | 1.06 | 85.05 | 0.84 | 174 | **0.77** | **0.36** | **31.06** | **0.03** | **264** |
| | Shrub/scrub | 0.88 | 0.17 | 56.64 | -0.04 | 597 | 0.86 | 0.18 | 57.23 | -0.05 | 595 | **0.91** | **0.07** | **21.09** | **0.01** | **876** |
| | Woody wetlands | 0.84 | 0.66 | 35.15 | 0.18 | 300 | 0.86 | 0.64 | 34.53 | 0.21 | 298 | **0.81** | **0.57** | **31.60** | **0.02** | **439** |
| FAPAR | Cultivated crops | 0.91 | 0.07 | 26.19 | -0.06 | 172 | 0.89 | 0.07 | 28.65 | -0.07 | 172 | **0.87** | **0.04** | **16.04** | **0.01** | **260** |
| | Deciduous broadleaf | 0.82 | 0.10 | 16.95 | -0.03 | 637 | 0.84 | 0.10 | 15.97 | -0.02 | 641 | **0.88** | **0.08** | **13.49** | **0.00** | **877** |
| | Evergreen broadleaf | 0.64 | 0.10 | 13.64 | -0.07 | 178 | 0.57 | 0.09 | 12.49 | -0.04 | 175 | **0.46** | **0.09** | **11.65** | **-0.02** | **264** |
| | Evergreen needleleaf | **0.51** | **0.07** | **13.30** | **0.00** | **357** | **0.56** | **0.07** | **12.17** | **0.00** | **358** | 0.42 | 0.09 | 16.05 | 0.00 | 542 |
| | Grasslands | 0.96 | 0.05 | 18.27 | -0.04 | 300 | 0.96 | 0.06 | 19.32 | -0.04 | 299 | **0.96** | **0.04** | **12.35** | **0.00** | **445** |
| | Mixed forest | 0.70 | 0.14 | 21.93 | -0.02 | 430 | 0.75 | 0.12 | 20.25 | -0.01 | 435 | **0.82** | **0.09** | **14.95** | **-0.01** | **589** |
| | Pasture/hay | **0.83** | **0.07** | **13.94** | **0.04** | **174** | **0.84** | **0.07** | **14.56** | **0.04** | **174** | 0.75 | 0.08 | 15.67 | 0.00 | 264 |
| | Shrub/scrub | 0.81 | 0.08 | 44.77 | -0.06 | 597 | 0.82 | 0.08 | 45.60 | -0.06 | 595 | **0.89** | **0.03** | **16.17** | **0.00** | **876** |
| | Woody wetlands | **0.82** | **0.08** | **15.07** | **-0.01** | **300** | **0.80** | **0.08** | **15.80** | **0.00** | **298** | **0.80** | **0.08** | **15.04** | **-0.01** | **439** |

sensitive to slightly different quantities. For example, the classification approach adopted for downwards-facing DHP images is predominantly sensitive to pixels that are green in colour (Meyer and Neto, 2008), and is therefore most related to green FIPAR (Tao et al., 2015), which may underestimate FAPAR for shrub/scrub canopies where greater amounts of yellowing foliage is present, causing the EO products to appear positively biased. Despite not being characteristically green in colour, this foliage may still present a strong signal in the near-infrared wavelengths that the EO product retrieval schemes are sensitive to. It is also worth noting that for sparse canopies with bright soils, using simulated data, Gobron et al. (2006) found that in situ measurements of FIPAR will underestimate FAPAR to some degree. Combined, these factors could explain why the EO products appeared to be subject to overestimation over shrub/scrub vegetation. Similarly, over forests, it is known that two-flux FIPAR (as estimated by DHP) may overestimate four-flux FAPAR (as retrieved by the EO products) (Putzenlechner et al., 2020). An additional source of uncertainty relates to temporal differences between the various datasets considered in our study. Retrievals from SL2P and the CGLS 300 m V1 product are defined as instantaneous FAPAR under clear sky conditions at 10:00 local solar time (Baret et al., 2016; Weiss and Baret, 2016), corresponding closely to the in situ reference measurements, which represent instantaneous black-sky FIPAR at 10:00 (also equivalent to 14:00) local solar time (Appendix B). On the other hand, the MOD15A2H and VNP15A2H products represent instantaneous FAPAR under clear sky conditions at the time of the satellite overpass (approximately 10:30 local solar time for Terra and 13:30 local solar time for S-NPP). These differences may lead to a slight bias that was not explicitly accounted for.

In terms of LAI, because we could not distinguish between foliage and other canopy elements such as stems and branches in the upwards-facing DHP images, the resulting PAI estimates are likely to overestimate in situ LAI in the case of woody species. Chen (1996) and Gower et al. (1999) suggest overestimation of between 5% and 35% is typical, whilst a similar impact is likely for FIPAR. An additional source of uncertainty is related to the correction for foliage clumping. Woodgate et al. (2017) demonstrate that the clumping correction method adopted in this study is sensitive to the size of the azimuth cells over which it is computed, finding that over a simulated eucalypt forest, the method of Leblanc et al. (2005) offered better performance, agreeing to within 25% to 30% of reference PAI values. Having said this, Leblanc and Fournier (2014) report similar performance for both methods using an azimuth cell size close to that adopted in this study (Appendix B). It is also worth noting that some studies have suggested the effects of woody area and foliage clumping may be partially compensatory (Fang et al., 2019a; Schlerf et al., 2005).

### 5.2. Utility of the GBOV in situ reference measurements

Leveraging routine data collection by NEON and operational processing chains developed within the GBOV project, over 70,000 raw DHP images were processed to provide 4,178 in situ PAI and FIPAR reference measurements, each accompanied by quality indicators. Although not explicitly considered in this paper, FCOVER data were also produced and are available to the community. When 3,437 quality controlled in situ reference measurements are compared, the typical relationship exhibited between PAI and FIPAR provides reassurance that the derived data are consistent with both empirical observations and the physical principles of radiation transfer in vegetation canopies. Notably, by using a common processing chain alongside standardised instruments and data collection protocols, the GBOV in situ reference measurements avoid some of the inconsistencies associated with previous datasets used for LAI and FAPAR product evaluation. By making use of both upwards- and downwards-facing DHP data, we were able to assess the impact of neglecting the understory layer in forest environments, which led to an RMSD of 0.76 for PAI and 0.11 for FIPAR.

Using procedures based on the recommendations of the CEOS WGCV LPV sub-group, an improved upscaling framework was developed and applied, resulting in high spatial resolution PAI and FIPAR reference maps covering twenty sites between 2015 and 2018. Our results complement the 242 samples already available in the DIRECT 2.0 database, and will enable new and existing products to progress towards stage three of the CEOS WGCV LPV hierarchy. Notwithstanding this fact, increased consistency with the considered EO products could be achieved in future work by applying additional corrections to the in situ reference measurements. The influence of woody area is a key source of uncertainty in forest environments, and to enable its quantification and correction, we recommend that future DHP acquisition protocols should incorporate a) leaf-off measurements, or b) the collection of images captured at multiple exposures to allow foliage to be distinguished from other canopy elements such as stems and branches (Woodgate et al., 2016). A further refinement could involve the use of near-infrared cameras, which might better discriminate foliage from other plant material (Baret et al., 1993; Osmond, 2009), although commercially availability of such systems is currently limited. Additionally, given the associated uncertainties reported over some vegetation types (Woodgate et al., 2017), alternative methods to correct

for foliage clumping should also be explored. To ensure their continued utility, the GBOV in situ reference measurements should also be updated when new raw data are made available.

As with other evaluations of moderate spatial resolution EO products, our results are dependent on the ability of the upscaling approach to adequately represent site-scale variability in vegetation condition. Although an improved RTM-based upscaling approach was adopted in our analysis, further refinements, including the grading of in situ reference measurements based on their spatial representativeness, have been successfully applied in recent studies (Xu et al., 2018). Future work should investigate whether such methods can be applied to produce more accurate high spatial resolution reference maps from GBOV in situ reference measurements. Additionally, the high spatial resolution maps could themselves be used to identify shortcomings in existing in situ spatial and temporal sampling. Finally, using a version of SL2P also compatible with Landsat 8 Operational Land Imager (OLI) data (Djamai et al., 2019), our upscaling approach could be extended to cover the full range of available in situ measurements and be implemented in a future release of the GBOV dataset.

Although the twenty NEON sites selected in the first phase of the project cover a wide range of vegetation types, there is a need to expand the dataset beyond the United States to improve geographical representativeness. In the first instance, this may be achieved by incorporating data from additional NEON sites and other environmental monitoring networks such as TERN and ICOS as they move into maturity. To further advance this objective, the next phase of the GBOV project plans to establish and upgrade additional field sites over Europe, Africa, and Oceania, with a particular focus on currently underrepresented areas such as the tropical and semiarid regions (Fang et al., 2019a). In addition to routine field sampling, these sites will feature automated instruments (Brown et al., 2020) to improve characterisation of temporal dynamics. Although currently beyond the scope of the GBOV project, activities to reconcile existing in situ reference measurement datasets could also be envisaged in future work (for example by harmonising previously collected data using a common processing chain, and ascribing uncertainties to the various measurement protocols). To be most effective, coordinated effort from the international community will be required in this respect.

## 6. Conclusions

Although existing in situ reference measurement datasets have proven valuable for the evaluation of EO derived LAI and FAPAR products, inconsistencies due to different instruments and data collection protocols have proven problematic. Furthermore, reliance on individual field campaigns has limited progress towards stage three of the CEOS WGCV LPV hierarchy. By processing standardised and routine data collected at twenty NEON sites, 4,178 in situ reference measurements have been made available through the GBOV project (these data can be obtained at https://land.copernicus.eu/global/gbov/), providing substantial progress in this respect.

Intercomparison of three global LAI and FAPAR products revealed strong agreement between the MOD15A2H and VNP15A2H products, providing users with confidence that continuity will be ensured when the MODIS instruments reach the end of their operational lives. In terms of product evaluation, the CGLS 300 m V1 product demonstrated the best agreement with reference data, with 92% of LAI and 89% of FAPAR retrievals meeting uncertainty requirements, highlighting the successful function of its retrieval approach, which aims to exploit the respective strengths of several existing EO products.

Whilst the number of sites at which GBOV in situ reference measurements are available is somewhat limited, the consistency and size of the dataset are key advantages that complement existing databases, as is the availability of data throughout the phenological cycle, which will facilitate progress towards stage three of the CEOS WGCV LPV hierarchy. To ensure they continue to prove useful for product evaluation, future work should focus on updating the GBOV in situ reference measurements as new raw data are released. The implementation of additional corrections should also be considered, whilst the geographical representativeness of the dataset should be improved by incorporating additional sites and other environmental monitoring networks as they become more mature.

## Acknowledgements

The authors are grateful to Fernando Camacho, Roselyne Lacaze and Richard Fernandes for feedback on an earlier version of the GBOV dataset. The authors also thank the Associate Editor Youngryel Ryu and the four anonymous reviewers for their constructive comments, which helped to substantially improve the manuscript. This study has been undertaken using data from the Global Component of the European Union's Copernicus Land Monitoring Service. European Commission Joint Research Centre FWC 932059. The authors are grateful to NASA and the Oak Ridge National Laboratory (ORNL) Distributed Active Archive Centre (DAAC) for access to MODIS and VIIRS land product subsets. The National Ecological Observatory Network is a program sponsored by the National Science Foundation and operated under cooperative agreement by Battelle Memorial Institute. This material is based in part upon work supported by the National Science Foundation through the NEON Program.

## Declaration of Competing Interest

The authors declare that they have no known competing financial interests or personal relationships that could have appeared to influence the work reported in this paper.

## Appendix A. Spatial representativeness

Using 30 m land cover data from the 2016 NLCD (Homer et al., 2020), we assessed spatial representativeness by calculating the percentage of each land cover class within a 1.5 km × 1.5 km area centred on the location of each site's tower. This extent was selected to match the area over which product performance was assessed (Section 3.6). Most of the investigated sites were dominated by a single land cover class, which accounted for the majority of the 1.5 km × 1.5 km area (Table A1). However, at seven sites, the modal land cover class accounted for less than 50% of the 1.5 km x 1.5 km area. Note that four of these seven sites (i.e. BART, BLAN, HARV, and TALL) were dominated by two related land cover classes (e.g. deciduous forest and mixed forest, deciduous forest and evergreen forest, or cultivated crops and pasture/hay).

Table A1

Percentage of each land cover class within a 1.5 km × 1.5 km area centred on the location of each site. Land cover data from the 2016 NLCD (Homer et al., 2020), with the exception of GUAN, where data are only available from the 2001 NLCD. The modal land cover type at each site is shown in bold. For clarity, only classes accounting for ≥ 1% are shown.

| | Site | | | | | | | | | | | | | | | | | | | |
|---|---|---|---|---|---|---|---|---|---|---|---|---|---|---|---|---|---|---|---|---|
| Land cover | BART | BLAN | CPER | DSNY | GUAN | HARV | JERC | JORN | MOAB | NIWO | ONAQ | ORNL | OSBS | SCBI | SERC | STEI | STER | TALL | UNDE | WOOD |
| Open water | - | - | - | 1% | - | - | - | - | - | - | - | - | 2% | - | 1% | - | - | - | 1% | 9% |
| Developed, open space | 7% | 9% | 2% | 7% | - | - | 2% | - | 4% | - | - | 3% | 8% | - | 5% | 4% | 4% | 4% | 7% | 3% |
| Developed, low intensity | - | 1% | - | 4% | - | - | 1% | - | 1% | - | - | 4% | - | - | 1% | 1% | - | - | - | - |
| Developed, medium intensity | - | - | - | - | - | - | - | - | - | - | - | 6% | - | - | - | - | - | - | - | - |
| Developed, high intensity | - | - | - | - | - | - | - | - | - | - | - | 1% | - | - | - | - | - | - | - | - |
| Barren land | - | - | - | - | - | - | - | - | - | - | - | - | - | - | - | - | - | - | - | - |
| Deciduous forest | 40% | 9% | - | - | - | 27% | 7% | - | - | - | - | **80%** | 1% | **98%** | **63%** | 17% | - | **42%** | 31% | 2% |
| Evergreen forest | 6% | - | - | - | **98%** | 14% | **44%** | - | - | 5% | - | 1% | **47%** | - | 4% | - | - | 40% | - | - |
| Mixed forest | **43%** | 6% | - | - | - | **41%** | 9% | - | - | - | - | 2% | - | 1% | 4% | **56%** | - | 14% | 3% | - |
| Shrub/scrub | 1% | - | 25% | - | - | - | 1% | **84%** | **86%** | **54%** | **85%** | **-** | 32% | - | - | 4% | - | - | - | - |
| Grassland/herbaceous | - | - | **73%** | 1% | 2% | - | 7% | 16% | 8% | 41% | 15% | - | 6% | - | - | - | 15% | - | - | **61%** |
| Pasture/hay | - | **42%** | - | 34% | - | - | 1% | - | - | - | - | 3% | 5% | - | 1% | - | - | - | - | 8% |
| Cultivated crops | 2% | 33% | - | - | - | - | 20% | - | - | - | - | - | - | - | 5% | - | **81%** | - | - | 11% |
| Woody wetlands | - | - | - | **47%** | - | 18% | 8% | - | - | - | - | - | - | - | 16% | 17% | - | - | **56%** | - |
| Emergent herbaceous wetlands | - | - | - | 7% | - | - | - | - | - | - | - | - | - | - | - | 1% | - | - | 1% | 7% |

## Appendix B. Deriving PAI and FIPAR

Before deriving PAI and FIPAR, images underwent quality control. ESUs with images demonstrating fixed pattern noise, overexposure, colour balance issues, variable illumination, or foreign objects within the field-of-view were discarded, as were ESUs with less than 12 images or images acquired in lossy formats. Similarly, forest ESUs at which no understory measurements were acquired were also discarded following Camacho et al. (2013) and Weiss et al. (2014). Once quality controlled, steps were then taken to increase image contrast in order to improve the subsequent classification results. Following the approach recommended by Macfarlane et al. (2014), raw images were first gamma corrected, before then being contrast stretched so that 1% of pixels at the high and low ends of the image histogram were saturated. The resultant images were stored in 8-bit form for further analysis.

To calculate PAI and FIPAR from the DHP images, pixels were classified as belonging to the vegetation canopy or its background (i.e. the sky for upwards-facing images and the soil for downwards-facing images). Although alternative methods to process upwards-facing images have been described in recent years, including the reconstruction of a sky reference image to enable the estimation of sub-pixel gap fraction (Hwang et al., 2016; Lang et al., 2010, 2017), we adopted a binary classification to maintain a consistent approach for both upwards- and downwards-facing images. Once classified, images were divided into zenith rings of 10°, and each zenith ring into a further thirty-six azimuth cells of 10°. In the case of downwards-facing images, a 90° azimuthal mask was applied to remove the operator from the field-of-view. Within each ESU and angular bin, the gap fraction was computed over all twelve images as the ratio of number of pixels classified as the background to the total number of pixels.

From estimates of gap fraction, PAI was determined according to Warren-Wilson (1963) as

$$PAI = -2\ \overline{\ln P(\theta_{57.5^\circ})}\cos\theta_{57.5^\circ} = \frac{-\overline{\ln P(\theta_{57.5^\circ})}}{0.93}$$

where $P(\theta_{57.5^\circ})$ is the gap fraction in a zenith ring centred at the hinge angle of 57.5° ( ± 5°). When compared to Miller's (1967) integral, Leblanc and Fournier (2014) suggest that Warren-Wilson's (1963) method provides more stable estimates of PAI under canopies with different leaf angle distributions. Note that by calculating the mean of the natural logarithm of gap fraction values over all azimuth cells and images, we accounted for the effects of within- and between-crown foliage clumping according to Lang and Yueqin (1986). Whilst several alternative foliage clumping correction approaches are available (Chen and Cihlar, 1995; Leblanc, 2002; Leblanc et al., 2005), we adopted the method of Lang and Yueqin (1986) as it is the approach implemented in CAN-EYE (Weiss and Baret, 2017) – one of the most widely used DHP analysis packages (Claverie et al., 2013; Djamai et al., 2019; Fang et al., 2018; Jay et al., 2018; Origo et al., 2017; Verger et al., 2011), and the primary tool used to process DHP data within the CEOS WGCV LPV sub-group (Weiss et al., 2014). Using three-dimensional forest simulations, Leblanc and Fournier (2014) evaluated several foliage clumping correction approaches, and whilst the method of Leblanc et al. (2005) was found to be the best performing, Lang and Yueqin's (1986) approach yielded similar results when calculated using an azimuth cell size of 15° (both methods led to an RMSD in PAI of between 1.0 and 1.1). It is worth noting that freely-available packages implementing the approach of Leblanc et al. (2005) are currently unsuitable for downwards-facing DHP images (Leblanc, 2008), which were a key component of our study.

FIPAR was calculated according to the instantaneous black-sky definition at 10:00 (also equivalent to 14:00) local solar time. Under the assumption of a black (i.e. completely absorbing) canopy, instantaneous black-sky FIPAR can be derived as

$$FIPAR = 1 - \overline{P(\theta_{SZA})}$$

where $\overline{P(\theta_{SZA})}$ is the mean gap fraction of a zenith ring centred on the solar zenith angle at 10:00 local solar time ( ± 5°).

At sites where both an understory and overstory was present, in situ reference measurements were derived from both upwards- and downwards-facing DHP images, and were combined to obtain a single value. In the case of PAI, the combination was additive, such that

$$PAI = PAI_{up} + PAI_{down}$$

where $PAI_{up}$ and $PAI_{down}$ are PAI values derived from upwards- and downwards-facing DHP images, respectively. In the case of FIPAR, the combined value was obtained as

$$FIPAR = FIPAR_{up} + (1 - FIPAR_{up})\, FIPAR_{down}$$

where $FIPAR_{up}$ and $FIPAR_{down}$ are FIPAR values derived from upwards- and downwards-facing DHP images, respectively.

*Appendix C. Seasonal and annual variations in product performance*

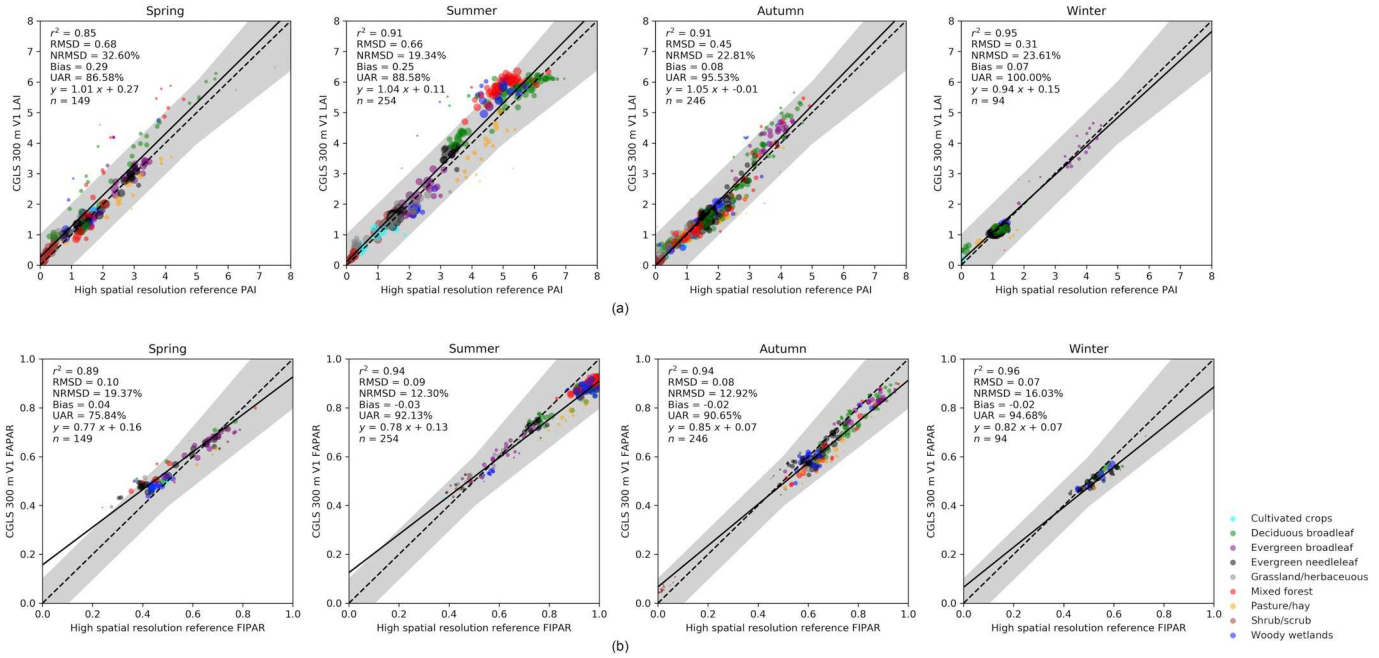


**Fig. C1.** Evaluation of CGLS 300 m V1 LAI (a) and FAPAR (b) products against high spatial resolution reference maps, by meteorological season. The dashed line represents a 1:1 relationship, whilst the shaded grey area represents the uncertainty requirements. Points are scaled by their density.

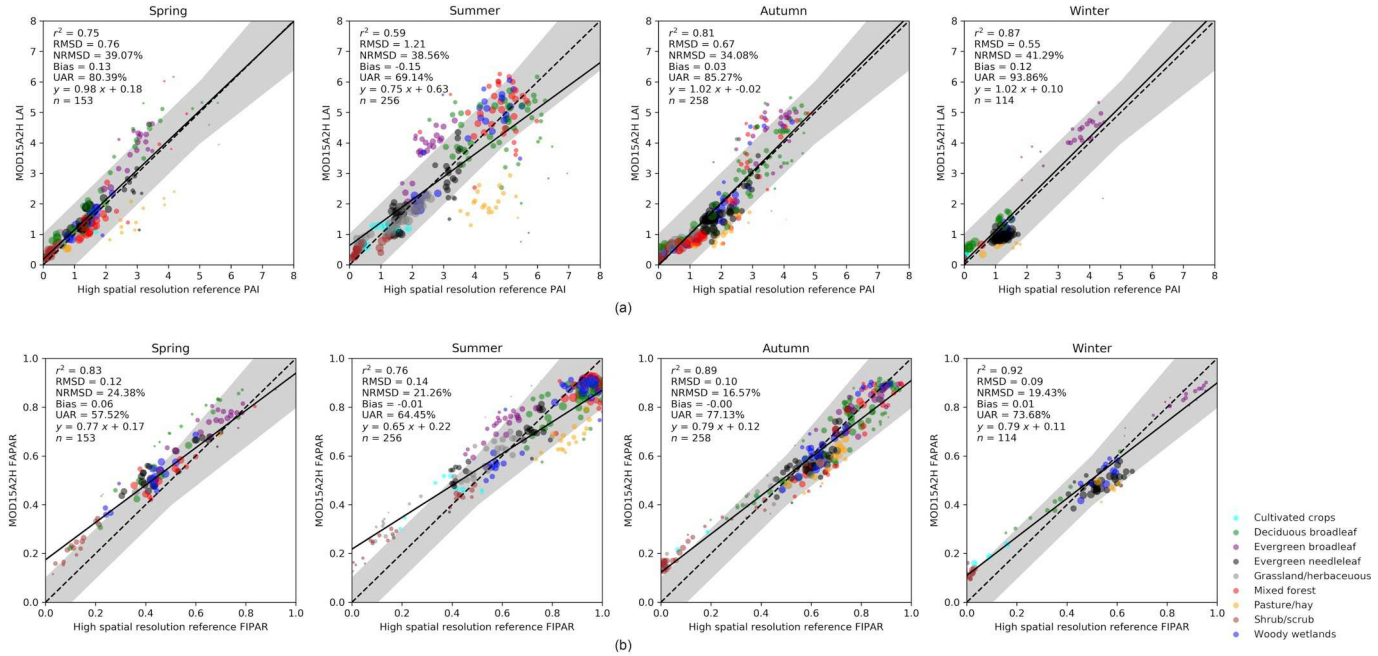


**Fig. C2.** Evaluation of MOD15A2H LAI (a) and FAPAR (b) products against high spatial resolution reference maps, by meteorological season. The dashed line represents a 1:1 relationship, whilst the shaded grey area represents the uncertainty requirements. Points are scaled by their density.

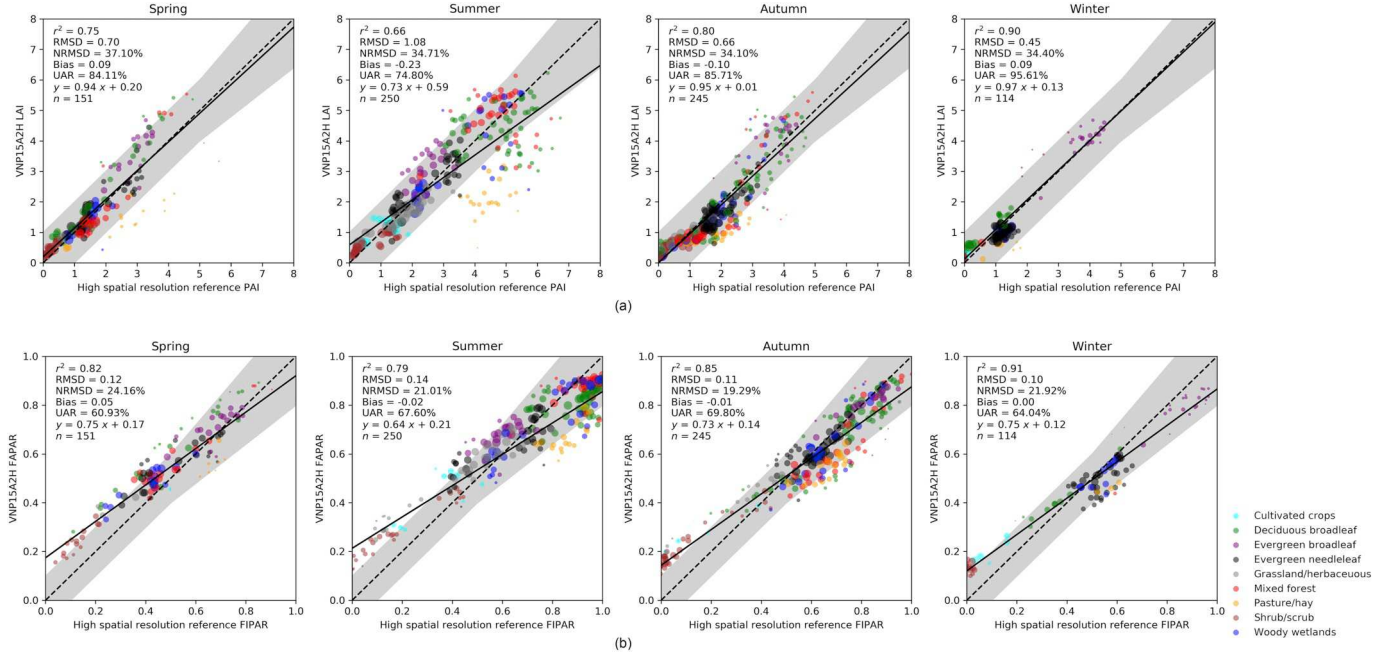


**Fig. C3.** Evaluation of VNP15A2H LAI (a) and FAPAR (b) products against high spatial resolution reference maps, by meteorological season. The dashed line represents a 1:1 relationship, whilst the shaded grey area represents the uncertainty requirements. Points are scaled by their density.

Table C1
Evaluation against high spatial resolution reference maps, by year. Note that a different number of points were available for each product due to differences in temporal resolution, the time period covered, and availability of valid data. The products with the lowest RMSD for each land cover type are shown in bold.

| | | CGLS 300 m V1 | | | | | | MOD15A2H | | | | | | VNP15A2H | | | | | |
|---|---|---|---|---|---|---|---|---|---|---|---|---|---|---|---|---|---|---|---|
| | Year | $r^2$ | RMSD | NRMSD (%) | Bias | UAR (%) | *n* | $r^2$ | RMSD | NRMSD (%) | Bias | UAR (%) | *n* | $r^2$ | RMSD | NRMSD (%) | Bias | UAR (%) | *n* |
| LAI | 2015 | **0.96** | **0.29** | **18.64** | **0.09** | **100.00** | **27** | 0.86 | 0.56 | 35.59 | 0.13 | 92.59 | 27 | 0.86 | 0.50 | 32.03 | 0.00 | 92.59 | 27 |
| | 2016 | **0.90** | **0.61** | **24.31** | **0.12** | **88.31** | **154** | 0.66 | 0.94 | 40.42 | -0.10 | 78.77 | 146 | 0.72 | 0.86 | 36.87 | -0.10 | 79.87 | 149 |
| | 2017 | **0.91** | **0.60** | **25.31** | **0.19** | **91.39** | **244** | 0.75 | 0.89 | 40.81 | 0.07 | 79.69 | 256 | 0.76 | 0.83 | 38.64 | -0.10 | 82.94 | 252 |
| | 2018 | **0.93** | **0.54** | **21.87** | **0.20** | **93.10** | **318** | 0.74 | 0.88 | 37.81 | -0.01 | 81.25 | 352 | 0.78 | 0.79 | 34.52 | -0.06 | 84.64 | 332 |
| FAPAR | 2015 | **0.94** | **0.07** | **13.62** | **-0.03** | **81.48** | **27** | 0.79 | 0.11 | 19.56 | 0.01 | 66.67 | 27 | 0.82 | 0.10 | 18.97 | 0.00 | 70.37 | 27 |

(*continued on next page*)

Table C1 (*continued*)

| | CGLS 300 m V1 | | | | | | MOD15A2H | | | | | | VNP15A2H | | | | | |
|---|---|---|---|---|---|---|---|---|---|---|---|---|---|---|---|---|---|---|
| 2016 | **0.92** | **0.09** | **14.34** | **-0.03** | **88.96** | **154** | 0.82 | 0.11 | 18.92 | -0.01 | 67.81 | 146 | 0.84 | 0.11 | 18.79 | -0.01 | 68.46 | 149 |
| 2017 | **0.94** | **0.09** | **14.87** | **-0.01** | **87.30** | **244** | 0.87 | 0.12 | 21.19 | 0.02 | 63.67 | 256 | 0.86 | 0.13 | 23.12 | 0.00 | 61.11 | 252 |
| 2018 | **0.93** | **0.08** | **13.55** | **0.00** | **89.97** | **318** | 0.83 | 0.12 | 20.38 | 0.01 | 71.02 | 352 | 0.83 | 0.12 | 21.13 | 0.00 | 65.96 | 332 |

Conceptualization, L.A.B. and J.D.; methodology, L.A.B.; software, L.A.B., H.M., J.P. and G.B.; validation, L.A.B., H.M., J.P., G.B., C.L. and J.D.; formal analysis, L.A.B.; investigation, L.A.B.; resources, L.A.B., C.M., C.L., G.B. and J.D.; data curation, L.A.B., C.M., C.L. and G.B.; writing—original draft preparation, L.A.B.; writing—review and editing, L.A.B., C.M., H.M., J.P., N.G. and J.D.; visualization, L.A.B. and C.M.; supervision, L.A.B., C.L., N.G., M.C. and J.D.; project administration, C.L., N.G and M.C.; funding acquisition, L.A.B., C.L. and J.D.

## References


Abuelgasim, A.A., Fernandes, R.A., Leblanc, S.G., 2006. Evaluation of national and global LAI products derived from optical remote sensing instruments over Canada. IEEE Trans. Geosci. Remote Sens. 44, 1872–1884. https://doi.org/10.1109/TGRS.2006.874794.

Bacour, C., Baret, F., Béal, D., Weiss, M., Pavageau, K., 2006. Neural network estimation of LAI, fAPAR, fCover and LAIxCab, from top of canopy MERIS reflectance data: Principles and validation. Remote Sens. Environ. 105, 313–325. https://doi.org/10.1016/j.rse.2006.07.014.

Baret, F., Buis, S., 2008. Estimating canopy characteristics from remote sensing observations: review of methods and associated problems. In: Liang, S. (Ed.), Advances in Land Remote Sensing: System, Modeling, Inversion and Application. Springer, Dordrecht, Netherlands, pp. 173–201. https://doi.org/10.1007/978-1-4020-6450-0_7.

Baret, F., Andrieu, B., Folmer, J.C., Hanocq, J.F., Sarrouy, C., 1993. Gap fraction measurement using hemispherical infrared photographies and its use to evaluate PAR interception efficiency. In: Varlet-Grancher, C., Bonhomme, R., Sinoquet, H. (Eds.), Crop Structure and Light Microclimate: Characterization and Applications. Institut National de la Recherche Agronomique, Paris, France, pp. 359–371.

Baret, F., Weiss, M., Allard, D., Garrigues, S., Leroy, M., Jeanjean, H., Fernandes, R., Myneni, R., Privette, J., Morisette, J., Bohbot, H., 2005. VALERI: A Network of Sites and a Methodology for the Validation of Medium Spatial Resolution Land Satellite Products. Institut National de la Recherche Agronomique, Avignon, France.

Baret, F., Hagolle, O., Geiger, B., Bicheron, P., Miras, B., Huc, M., Berthelot, B., Niño, F., Weiss, M., Samain, O., Roujean, J.L., Leroy, M., 2007. LAI, fAPAR and fCover CYCLOPES global products derived from VEGETATION. Remote Sens. Environ. 110, 275–286. https://doi.org/10.1016/j.rse.2007.02.018.

Baret, F., Weiss, M., Lacaze, R., Camacho, F., Makhmara, H., Pacholcyzk, P., Smets, B., 2013. GEOV1: LAI and FAPAR essential climate variables and FCOVER global time series capitalizing over existing products. Part 1: principles of development and production. Remote Sens. Environ. 137, 299–309. https://doi.org/10.1016/j.rse.2012.12.027.

Baret, F., Weiss, M., Verger, A., Smets, B., 2016. ATBD for LAI, FAPAR and FCOVER from PROBA-V Products at 300m Resolution (GEOV3), 1.73. Institut National de la Recherche Agronomique, Avignon, France.

Beckschäfer, P., Seidel, D., Kleinn, C., Xu, J., 2013. On the exposure of hemispherical photographs in forests. iForest - Biogeosciences For. 6, 228–237. https://doi.org/10.3832/ifor0957-006.

Bréda, N.J.J., 2003. Ground-based measurements of leaf area index: a review of methods, instruments and current controversies. J. Exp. Bot. 54, 2403–2417. https://doi.org/10.1093/jxb/erg263.

Brown, L.A., Dash, J., Lidon, A.L., Lopez-Baeza, E., Dransfeld, S., 2019. Synergetic exploitation of the Sentinel-2 missions for validating the Sentinel-3 Ocean and Land Color Instrument Terrestrial Chlorophyll Index over a vineyard dominated mediterranean environment. IEEE J. Sel. Top. Appl. Earth Obs. Remote Sens. 12, 2244–2251. https://doi.org/10.1109/JSTARS.2019.2899998.

Brown, L.A., Ogutu, B.O., Dash, J., 2019b. Estimating forest leaf area index and canopy chlorophyll content with Sentinel-2: an evaluation of two hybrid retrieval algorithms. Remote Sens. 11, 1752. https://doi.org/10.3390/rs11151752.

Brown, L.A., Ogutu, B.O., Dash, J., 2020. Tracking forest biophysical properties with automated digital repeat photography: a fisheye perspective using digital hemispherical photography from below the canopy. Agric. For. Meteorol. 287, 107944. https://doi.org/10.1016/j.agrformet.2020.107944.

Calders, K., Origo, N., Disney, M., Nightingale, J., Woodgate, W., Armston, J., Lewis, P., 2018. Variability and bias in active and passive ground-based measurements of effective plant, wood and leaf area index. Agric. For. Meteorol. 252, 231–240. https://doi.org/10.1016/j.agrformet.2018.01.029.

Camacho, F., Cernicharo, J., Lacaze, R., Baret, F., Weiss, M., 2013. GEOV1: LAI, FAPAR essential climate variables and FCOVER global time series capitalizing over existing products. Part 2: validation and intercomparison with reference products. Remote Sens. Environ. 137, 310–329. https://doi.org/10.1016/j.rse.2013.02.030.

Campos-Taberner, M., García-Haro, F., Confalonieri, R., Martínez, B., Moreno, Á., Sánchez-Ruiz, S., Gilabert, M., Camacho, F., Boschetti, M., Busetto, L., 2016. Multitemporal monitoring of plant area index in the Valencia rice district with PocketLAI. Remote Sens. 8, 202. https://doi.org/10.3390/rs8030202.

Canisius, F., Fernandes, R., Chen, J., 2010. Comparison and evaluation of medium resolution imaging spectrometer leaf area index products across a range of land use. Remote Sens. Environ. 114, 950–960. https://doi.org/10.1016/j.rse.2009.12.010.

CEOS WGCV LPV, 2017. Dataset Description [WWW Document]. URL. http://calvalportal.ceos.org/web/olive/site-description (accessed 5.28.19).

CGLS, 2017. Leaf Area Index [WWW Document]. URL. https://land.copernicus.eu/global/products/lai (accessed 5.28.19).

Chen, J.M., 1996. Optically-based methods for measuring seasonal variation of leaf area index in boreal conifer stands. Agric. For. Meteorol. 80, 135–163. https://doi.org/10.1016/0168-1923(95)02291-0.

Chen, J.M., Cihlar, J., 1995. Plant canopy gap-size analysis theory for improving optical measurements of leaf-area index. Appl. Opt. 34, 6211–6222. https://doi.org/10.1364/AO.34.006211.

Claverie, M., Vermote, E.F., Weiss, M., Baret, F., Hagolle, O., Demarez, V., 2013. Validation of coarse spatial resolution LAI and FAPAR time series over cropland in southwest France. Remote Sens. Environ. 139, 216–230. https://doi.org/10.1016/j.rse.2013.07.027.

Cohen, W.B., Justice, C.O., 1999. Validating MODIS terrestrial ecology products. Remote Sens. Environ. 70, 1–3. https://doi.org/10.1016/S0034-4257(99)00053-X.

De Kauwe, M.G., Disney, M.I., Quaife, T., Lewis, P., Williams, M., 2011. An assessment of the MODIS collection 5 leaf area index product for a region of mixed coniferous forest. Remote Sens. Environ. 115, 767–780. https://doi.org/10.1016/j.rse.2010.11.004.

Djamai, N., Fernandes, R., Weiss, M., McNairn, H., Goïta, K., 2019. Validation of the Sentinel Simplified Level 2 Product Prototype Processor (SL2P) for mapping cropland biophysical variables using Sentinel-2/MSI and Landsat-8/OLI data. Remote Sens. Environ. 225, 416–430. https://doi.org/10.1016/j.rse.2019.03.020.

Duveiller, G., Weiss, M., Baret, F., Defourny, P., 2011. Retrieving wheat Green Area Index during the growing season from optical time series measurements based on neural network radiative transfer inversion. Remote Sens. Environ. 115, 887–896. https://doi.org/10.1016/j.rse.2010.11.016.

ESA, 2019. Fiducial Reference Measurements: FRM [WWW Document]. URL. https://earth.esa.int/web/sppa/activities/frm (accessed 3.8.19).

Fang, H., Wei, S., Liang, S., 2012. Validation of MODIS and CYCLOPES LAI products using global field measurement data. Remote Sens. Environ. 119, 43–54. https://doi.org/10.1016/j.rse.2011.12.006.

Fang, H., Jiang, C., Li, W., Wei, S., Baret, F., Chen, J.M., Garcia-Haro, J., Liang, S., Liu, R., Myneni, R.B., Pinty, B., Xiao, Z., Zhu, Z., 2013. Characterization and intercomparison of global moderate resolution leaf area index (LAI) products: analysis of climatologies and theoretical uncertainties. J. Geophys. Res. Biogeosciences 118, 529–548. https://doi.org/10.1002/jgrg.20051.

Fang, H., Ye, Y., Liu, W., Wei, S., Ma, L., 2018. Continuous estimation of canopy leaf area index (LAI) and clumping index over broadleaf crop fields: an investigation of the PASTIS-57 instrument and smartphone applications. Agric. For. Meteorol. 253–254, 48–61. https://doi.org/10.1016/j.agrformet.2018.02.003.

Fang, H., Baret, F., Plummer, S., Schaepman-Strub, G., 2019a. An overview of Global Leaf Area Index (LAI): methods, products, validation, and applications. Rev. Geophys. 57, 739–799. https://doi.org/10.1029/2018RG000608.

Fang, H., Zhang, Y., Wei, S., Li, W., Ye, Y., Sun, T., Liu, W., 2019b. Validation of global moderate resolution leaf area index (LAI) products over croplands in northeastern Chinas. Remote Sens. Environ. 233, 111377. https://doi.org/10.1016/j.rse.2019.111377.

Fensholt, R., Sandholt, I., Rasmussen, M.S., 2004. Evaluation of MODIS LAI, fAPAR and the relation between fAPAR and NDVI in a semi-arid environment using in situ measurements. Remote Sens. Environ. 91, 490–507. https://doi.org/10.1016/j.rse.2004.04.009.

Feret, J.-B., François, C., Asner, G.P., Gitelson, A.A., Martin, R.E., Bidel, L.P.R., Ustin, S.L., le Maire, G., Jacquemoud, S., 2008. PROSPECT-4 and 5: advances in the leaf optical properties model separating photosynthetic pigments. Remote Sens. Environ. 112, 3030–3043. https://doi.org/10.1016/j.rse.2008.02.012.

Fernandes, R., Plummer, S., Nightingale, J., Baret, F., Camacho, F., Fang, H., Garrigues, S., Gobron, N., Lang, M., Lacaze, R., Leblanc, S., Meroni, M., Martinez, B., Nilson, T., Pinty, B., Pisek, J., Sonnentag, O., Verger, A., Welles, J., Weiss, M., Widlowski, J.-L., Schaepman-Strub, G., Roman, M., Nickeson, J., 2014. Global Leaf Area Index product validation good practices. In: Fernandes, R., Plummer, S., Nightingale, J. (Eds.), Best Practice for Satellite-Derived Land Product Validation. Land Product Validation Subgroup (Committee on Earth Observation Satellites Working Group on Calibration and Validation), https://doi.org/10.5067/doc/ceoswgcv/lpv/lai.002.

Fuster, B., Sánchez-Zapero, J., Camacho, F., García-Santos, V., Verger, A., Lacaze, R.,

Weiss, M., Baret, F., Smets, B., 2020. Quality assessment of PROBA-V LAI, fAPAR and fCOVER Collection 300 m products of Copernicus Global Land Service. Remote Sens. 12, 1017. https://doi.org/10.3390/rs12061017.
Garrigues, S., Lacaze, R., Baret, F., Morisette, J.T., Weiss, M., Nickeson, J.E., Fernandes, R., Plummer, S., Shabanov, N.V., Myneni, R.B., Knyazikhin, Y., Yang, W., 2008a. Validation and intercomparison of global Leaf Area Index products derived from remote sensing data. J. Geophys. Res. 113, G02028. https://doi.org/10.1029/2007JG000635.
Garrigues, S., Shabanov, N.V., Swanson, K., Morisette, J.T., Baret, F., Myneni, R.B., 2008b. Intercomparison and sensitivity analysis of Leaf Area Index retrievals from LAI-2000, AccuPAR, and digital hemispherical photography over croplands. Agric. For. Meteorol. 148, 1193–1209. https://doi.org/10.1016/j.agrformet.2008.02.014.
GCOS, 2019. Essential Climate Variables [WWW Document]. URL. https://public.wmo.int/en/programmes/global-climate-observing-system/essential-climate-variables (accessed 5.2.19).
Gielen, B., Acosta, M., Altimir, N., Buchmann, N., Cescatti, A., Ceschia, E., Fleck, S., Hörtnagl, L., Klumpp, K., Kolari, P., Lohila, A., Loustau, D., Marañon-Jimenez, S., Manise, T., Matteucci, G., Merbold, L., Metzger, C., Moureaux, C., Montagnani, L., Nilsson, M.B., Osborne, B., Papale, D., Pavelka, M., Saunders, M., Simioni, G., Soudani, K., Sonnentag, O., Tallec, T., Tuittila, E.-S., Peichl, M., Pokorny, R., Vincke, C., Wohlfahrt, G., 2018. Ancillary vegetation measurements at ICOS ecosystem stations. Int. Agrophysics 32, 645–664. https://doi.org/10.1515/intag-2017-0048.
Glatthorn, J., Beckschäfer, P., 2014. Standardizing the protocol for hemispherical photographs: accuracy assessment of binarization algorithms. PLoS One 9, e111924. https://doi.org/10.1371/journal.pone.0111924.
Gobron, N., 2010. Ocean and Land Colour Instrument (OLCI) FAPAR and Rectified Channels over Terrestrial Surfaces Algorithm Theoretical Basis Document. European Commission Joint Research Centre, Ispra, Italy.
Gobron, N., Pinty, B., Aussedat, O., Chen, J.M., Cohen, W.B., Fensholt, R., Gond, V., Huemmrich, K.F., Lavergne, T., Mélin, F., Privette, J.L., Sandholt, I., Taberner, M., Turner, D.P., Verstraete, M.M., Widlowski, J.-L., 2006. Evaluation of fraction of absorbed photosynthetically active radiation products for different canopy radiation transfer regimes: methodology and results using Joint Research Center products derived from SeaWiFS against ground-based estimations. J. Geophys. Res. 111, D13110. https://doi.org/10.1029/2005JD006511.
Gower, S.T., Kucharik, C.J., Norman, J.M., 1999. Direct and indirect estimation of Leaf Area Index, fAPAR, and net primary production of terrestrial ecosystems. Remote Sens. Environ. 70, 29–51. https://doi.org/10.1016/S0034-4257(99)00056-5.
Heiskanen, J., Rautiainen, M., Stenberg, P., Mõttus, M., Vesanto, V.-H., Korhonen, L., Majasalmi, T., 2012. Seasonal variation in MODIS LAI for a boreal forest area in Finland. Remote Sens. Environ. 126, 104–115. https://doi.org/10.1016/j.rse.2012.08.001.
Holben, B.N., 1986. Characteristics of maximum-value composite images from temporal AVHRR data. Int. J. Remote Sens. 7, 1417–1434. https://doi.org/10.1080/01431168608948945.
Homer, C., Dewitz, J., Jin, S., Xian, G., Costello, C., Danielson, P., Gass, L., Funk, M., Wickham, J., Stehman, S., Auch, R., Riitters, K., 2020. Conterminous United States land cover change patterns 2001–2016 from the 2016 National Land Cover Database. ISPRS J. Photogramm. Remote Sens. 162, 184–199. https://doi.org/10.1016/j.isprsjprs.2020.02.019.
Hwang, Y., Ryu, Y., Kimm, H., Jiang, C., Lang, M., Macfarlane, C., Sonnentag, O., 2016. Correction for light scattering combined with sub-pixel classification improves estimation of gap fraction from digital cover photography. Agric. For. Meteorol. 222, 32–44. https://doi.org/10.1016/j.agrformet.2016.03.008.
Iiames, J.S., Pilant, A.N., Lewis, T.E., 2004. In situ estimates of forest LAI for MODIS data validation. In: Lunetta, R.S., Lyon, J.G. (Eds.), Remote Sensing and GIS Accuracy Assessment. CRC Press, Boca Raton, Florida, United States, pp. 41–58.
ImagineS Consortium, 2016. Ground Data [WWW Document]. URL. http://fp7-imagines.eu/pages/services-and-products/ground-data.php (accessed 6.24.19).
Jay, S., Baret, F., Dutartre, D., Malatesta, G., Héno, S., Comar, A., Weiss, M., Maupas, F., 2018. Exploiting the centimeter resolution of UAV multispectral imagery to improve remote-sensing estimates of canopy structure and biochemistry in sugar beet crops. Remote Sens. Environ. https://doi.org/10.1016/j.rse.2018.09.011. 0–1.
Jonckheere, I., Fleck, S., Nackaerts, K., Muys, B., Coppin, P., Weiss, M., Baret, F., 2004. Review of methods for in situ leaf area index determination. Agric. For. Meteorol. 121, 19–35. https://doi.org/10.1016/j.agrformet.2003.08.027.
Kao, R.H., Gibson, C.M., Gallery, R.E., Meier, C.L., Barnett, D.T., Docherty, K.M., Blevins, K.K., Travers, P.D., Azuaje, E., Springer, Y.P., Thibault, K.M., McKenzie, V.J., Keller, M., Alves, L.F., Hinckley, E.-L.S., Parnell, J., Schimel, D., 2012. NEON terrestrial field observations: designing continental-scale, standardized sampling. Ecosphere 3https://doi.org/10.1890/ES12-00196.1. art115.
Karan, M., Liddell, M., Prober, S.M., Arndt, S., Beringer, J., Boer, M., Cleverly, J., Eamus, D., Grace, P., Van Gorsel, E., Hero, J.-M., Hutley, L., Macfarlane, C., Metcalfe, D., Meyer, W., Pendall, E., Sebastian, A., Wardlaw, T., 2016. The Australian SuperSite network: a continental, long-term terrestrial ecosystem observatory. Sci. Total Environ. 568, 1263–1274. https://doi.org/10.1016/j.scitotenv.2016.05.170.
Lacaze, R., Smets, B., Baret, F., Weiss, M., Ramon, D., Montersleet, B., Wandrebeck, L., Calvet, J.-C., Roujean, J.-L., Camacho, F., 2015. Operational 333m biophysical products of the Copernicus Global Land Service for agriculture monitoring. ISPRS - Int. Arch. Photogramm. Remote Sens. Spat. Inf. Sci. 53–56. https://doi.org/10.5194/isprsarchives-XL-7-W3-53-2015. XL-7/W3.
Lang, A.R.G., Yueqin, X., 1986. Estimation of leaf area index from transmission of direct sunlight in discontinuous canopies. Agric. For. Meteorol. 37, 229–243. https://doi.org/10.1016/0168-1923(86)90033-X.
Lang, M., Kuusk, A., Mõttus, M., Rautiainen, M., Nilson, T., 2010. Canopy gap fraction estimation from digital hemispherical images using sky radiance models and a linear conversion method. Agric. For. Meteorol. 150, 20–29. https://doi.org/10.1016/j.agrformet.2009.08.001.
Lang, M., Nilson, T., Kuusk, A., Pisek, J., Korhonen, L., Uri, V., 2017. Digital photography for tracking the phenology of an evergreen conifer stand. Agric. For. Meteorol. 246, 15–21. https://doi.org/10.1016/j.agrformet.2017.05.021.
Leblanc, S.G., 2002. Correction to the plant canopy gap-size analysis theory used by the Tracing Radiation and Architecture of Canopies instrument. Appl. Opt. 41, 7667. https://doi.org/10.1364/AO.41.007667.
Leblanc, S.G., 2008. DHP-TRACWin Manual. 1.0.3. ed. Natural Resources Canada, Québec, Canada.
Leblanc, S.G., Fournier, R.A., 2014. Hemispherical photography simulations with an architectural model to assess retrieval of leaf area index. Agric. For. Meteorol. 194, 64–76. https://doi.org/10.1016/j.agrformet.2014.03.016.
Leblanc, S.G., Chen, J.M., Fernandes, R., Deering, D.W., Conley, A., 2005. Methodology comparison for canopy structure parameters extraction from digital hemispherical photography in boreal forests. Agric. For. Meteorol. 129, 187–207. https://doi.org/10.1016/j.agrformet.2004.09.006.
Li, W., Weiss, M., Waldner, F., Defourny, P., Demarez, V., Morin, D., Hagolle, O., Baret, F., 2015. A generic algorithm to estimate LAI, FAPAR and FCOVER variables from SPOT4_HRVIR and landsat sensors: evaluation of the consistency and comparison with ground measurements. Remote Sens. 7, 15494–15516. https://doi.org/10.3390/rs71115494.
Macfarlane, C., Ryu, Y., Ogden, G.N., Sonnentag, O., 2014. Digital canopy photography: exposed and in the raw. Agric. For. Meteorol. 197, 244–253. https://doi.org/10.1016/j.agrformet.2014.05.014.
Martínez, B., García-Haro, F.J., Camacho-de Coca, F., 2009. Derivation of high-resolution leaf area index maps in support of validation activities: application to the cropland Barrax site. Agric. For. Meteorol. 149, 130–145. https://doi.org/10.1016/j.agrformet.2008.07.014.
Meier, C., Everhart, J., Jones, K., 2018. TOS Protocol and Procedure: Measurement of Leaf Area Index, K. ed. National Ecological Observatory Network, Boulder, Colorado, United States.
Meyer, G.E., Neto, J.C., 2008. Verification of color vegetation indices for automated crop imaging applications. Comput. Electron. Agric. 63, 282–293. https://doi.org/10.1016/j.compag.2008.03.009.
Miller, J., 1967. A formula for average foliage density. Aust. J. Bot. 15, 141–144. https://doi.org/10.1071/BT9670141.
Morisette, J.T., Baret, F., Privette, J.L., Myneni, R.B., Nickeson, J.E., Garrigues, S., Shabanov, N.V., Weiss, M., Fernandes, R.A., Leblanc, S.G., Kalacska, M., Sanchez-Azofeifa, G.A., Chubey, M., Rivard, B., Stenberg, P., Rautiainen, M., Voipio, P., Manninen, T., Pilant, A.N., Lewis, T.E., Iiames, J.S., Colombo, R., Meroni, M., Busetto, L., Cohen, W.B., Turner, D.P., Warner, E.D., Petersen, G.W., Seufert, G., Cook, R., 2006. Validation of global moderate-resolution LAI products: a framework proposed within the CEOS land product validation subgroup. IEEE Trans. Geosci. Remote Sens. 44, 1804–1817. https://doi.org/10.1109/TGRS.2006.872529.
Müller-Wilm, U., 2018. Sen2Cor Configuration and User Manual, 2nd ed. CS, Toulouse, France.
Myneni, R., Knyazikhin, Y., 2018. VIIRS/NPP Leaf Area Index/FPAR 8-Day L4 Global 500m SIN Grid V001 [WWW Document]. NASA EOSDIS L. Process. DAAC. https://doi.org/10.5067/VIIRS/VNP15A2H.001.
Myneni, R., Knyazikhin, Y., Park, T., 2015. MOD15A2H MODIS/Terra Leaf Area Index/FPAR 8-Day L4 Global 500m SIN Grid V006 [WWW Document]. NASA EOSDIS L. Process. DAAC. https://doi.org/10.5067/MODIS/MOD15A2H.006.
NASA, 2017. VIIRS NASA LAI/FPAR Product Validation: Version 1 Validation Statement [WWW Document]. URL. https://viirsland.gsfc.nasa.gov/Val/LAI_Fpar_Val.html (accessed 5.28.19).
Ogutu, B.O., Dash, J., Dawson, T.P., 2013. Developing a diagnostic model for estimating terrestrial vegetation gross primary productivity using the photosynthetic quantum yield and Earth Observation data. Glob. Chang. Biol. 19, 2878–2892. https://doi.org/10.1111/gcb.12261.
Origo, N., Calders, K., Nightingale, J., Disney, M., 2017. Influence of levelling technique on the retrieval of canopy structural parameters from digital hemispherical photography. Agric. For. Meteorol. 237–238, 143–149. https://doi.org/10.1016/j.agrformet.2017.02.004.
ORNL DAAC, 2018. MODIS and VIIRS Land Products Global Subsetting and Visualization Tool [WWW Document]. https://doi.org/10.3334/ORNLDAAC/1379.
Osmond, P., 2009. Application of Near-Infrared Hemispherical Photography to estimate leaf area index of urban vegetation. In: Proceedings of the Seventh International Conference on Urban Climate. International Association for Urban Climate, Yokohama, Japan.
Pasqualotto, N., Delegido, J., Van Wittenberghe, S., Rinaldi, M., Moreno, J., 2019. Multi-Crop Green LAI Estimation with a New Simple Sentinel-2 LAI Index (SeLI). Sensors 19, 904. https://doi.org/10.3390/s19040904.
Pueschel, P., Buddenbaum, H., Hill, J., 2012. An efficient approach to standardizing the processing of hemispherical images for the estimation of forest structural attributes. Agric. For. Meteorol. 160, 1–13. https://doi.org/10.1016/j.agrformet.2012.02.007.
Putzenlechner, B., Marzahn, P., Sanchez-Azofeifa, A., 2020. Accuracy assessment on the number of flux terms needed to estimate in situ fAPAR. International Journal of Applied Earth Observation and Geoinformation 88, 102061. https://doi.org/10.1016/j.jag.2020.102061.
Richardson, A.D., Keenan, T.F., Migliavacca, M., Ryu, Y., Sonnentag, O., Toomey, M., 2013. Climate change, phenology, and phenological control of vegetation feedbacks to the climate system. Agric. For. Meteorol. 169, 156–173. https://doi.org/10.1016/j.agrformet.2012.09.012.
Richter, K., Atzberger, C., Vuolo, F., Weihs, P., D'Urso, G., 2009. Experimental assessment of the Sentinel-2 band setting for RTM-based LAI retrieval of sugar beet and maize.

Can. J. Remote Sens. 35, 230–247. https://doi.org/10.5589/m09-010.
Richter, K., Atzberger, C., Hank, T.B., Mauser, W., 2012. Derivation of biophysical variables from Earth observation data: validation and statistical measures. J. Appl. Remote Sens. 6https://doi.org/10.1117/1.JRS.6.063557. 063557–1.
Sánchez-Zapero, J., Pérez, L., Fuster, B., 2018. Copernicus Global Land Operations "Vegetation and Energy" "CGLOPS-1" Scientific Quality Evaluation: LAI, FAPAR FCOVER Collection 300m Version 1, 1.10. ed. EOLAB, Valencia, Spain.
Schlerf, M., Atzberger, C., Hill, J., 2005. Remote sensing of forest biophysical variables using HyMap imaging spectrometer data. Remote Sens. Environ. 95, 177–194. https://doi.org/10.1016/j.rse.2004.12.016.
Sellers, P.J., Dickinson, R.E., Randall, D.A., Betts, A.K., Hall, F.G., Berry, J.A., Collatz, G.J., Denning, A.S., Mooney, H.A., Nobre, C.A., Sato, N., Field, C.B., Henderson-Sellers, A., 1997. Modeling the exchanges of energy, water, and carbon between continents and the atmosphere. Science 275, 502–509. https://doi.org/10.1126/science.275.5299.502. (80-. ).
SEN4SCI, 2011. Assessing Product Requirements for the Scientific Exploitation of the Sentinel Missions [WWW Document]. URL. http://www.geo.uzh.ch/microsite/sen4sci/ (accessed 1.29.20).
Swap, R.J., Privette, J.L., 1999. Overview of the Southern African Regional Science Initiative - SAFARI 2000. In: Proceedings of the 1999 IEEE International Geoscience and Remote Sensing Symposium. Institute of Electrical and Electronics Engineers, Hamburg, Germany.
Tan, B., Hu, J., Zhang, P., Huang, D., Shabanov, N., 2005. Validation of Moderate Resolution Imaging Spectroradiometer leaf area index product in croplands of Alpilles, France. J. Geophys. Res. 110, D01107. https://doi.org/10.1029/2004JD004860.
Tao, X., Liang, S., Wang, D., 2015. Assessment of five global satellite products of fraction of absorbed photosynthetically active radiation: intercomparison and direct validation against ground-based data. Remote Sens. Environ. 163, 270–285. https://doi.org/10.1016/j.rse.2015.03.025.
Tian, Y., Woodcock, C.E., Wang, Y., Privette, J.L., Shabanov, N.V., Zhou, L., Zhang, Y., Buermann, W., Dong, J., Veikkanen, B., Häme, T., Andersson, K., Ozdogan, M., Knyazikhin, Y., Myneni, R.B., 2002. Multiscale analysis and validation of the MODIS LAI product I. Uncertainty assessment. Remote Sens. Environ. 83, 414–430. https://doi.org/10.1016/S0034-4257(02)00047-0.
Vanino, S., Nino, P., De Michele, C., Falanga Bolognesi, S., D'Urso, G., Di Bene, C., Pennelli, B., Vuolo, F., Farina, R., Pulighe, G., Napoli, R., 2018. Capability of Sentinel-2 data for estimating maximum evapotranspiration and irrigation requirements for tomato crop in Central Italy. Remote Sens. Environ. 215, 452–470. https://doi.org/10.1016/j.rse.2018.06.035.
Verger, A., Baret, F., Camacho, F., 2011. Optimal modalities for radiative transfer-neural network estimation of canopy biophysical characteristics: Evaluation over an agricultural area with CHRIS/PROBA observations. Remote Sens. Environ. 115, 415–426. https://doi.org/10.1016/j.rse.2010.09.012.
Verger, A., Baret, F., Weiss, M., 2014. Near real-time vegetation monitoring at global scale. IEEE J. Sel. Top. Appl. Earth Obs. Remote Sens. 7, 3473–3481. https://doi.org/10.1109/JSTARS.2014.2328632.
Verhoef, W., Jia, L., Xiao, Q., Su, Z., 2007. Unified optical-thermal four-stream radiative transfer theory for homogeneous vegetation canopies. IEEE Trans. Geosci. Remote Sens. 45, 1808–1822. https://doi.org/10.1109/TGRS.2007.895844.
Verrelst, J., Camps-Valls, G., Muñoz-Marí, J., Rivera, J.P., Veroustraete, F., Clevers, J.G.P.W., Moreno, J., 2015. Optical remote sensing and the retrieval of terrestrial vegetation bio-geophysical properties – A review. ISPRS J. Photogramm. Remote Sens. 108, 273–290. https://doi.org/10.1016/j.isprsjprs.2015.05.005.
Vuolo, F., Dash, J., Curran, P.J., Lajas, D., Kwiatkowska, E., 2012. Methodologies and uncertainties in the use of the Terrestrial Chlorophyll Index for the Sentinel-3 mission. Remote Sens. 4, 1112–1133. https://doi.org/10.3390/rs4051112.
Warren-Wilson, J., 1963. Estimation of foliage denseness and foliage angle by inclined point quadrats. Aust. J. Bot. 11, 95–105.
Weiss, M., Baret, F., 2016. S2ToolBox Level 2 Products: LAI, FAPAR, FCOVER, 1.1. ed. Institut National de la Recherche Agronomique, Avignon, France.
Weiss, M., Baret, F., 2017. CAN-EYE V6.4.91 User Manual. Institut National de la Recherche Agronomique, Avignon, France.
Weiss, M., Baret, F., Smith, G.J., Jonckheere, I., Coppin, P., 2004. Review of methods for in situ leaf area index (LAI) determination Part II: Estimation of LAI, errors and sampling. Agric. For. Meteorol. 121, 37–53. https://doi.org/10.1016/j.agrformet.2003.08.001.
Weiss, M., Baret, F., Garrigues, S., Lacaze, R., 2007. LAI and fAPAR CYCLOPES global products derived from VEGETATION. Part 2: validation and comparison with MODIS collection 4 products. Remote Sens. Environ. 110, 317–331. https://doi.org/10.1016/j.rse.2007.03.001.
Weiss, M., Baret, F., Block, T., Koetz, B., Burini, A., Scholze, B., Lecharpentier, P., Brockmann, C., Fernandes, R., Plummer, S., Myneni, R., Gobron, N., Nightingale, J., Schaepman-Strub, G., Camacho, F., Sanchez-Azofeifa, A., 2014. On line validation exercise (OLIVE): A web based service for the validation of medium resolution land products. Application to FAPAR products. Remote Sens. 6, 4190–4216. https://doi.org/10.3390/rs6054190.
Woodgate, W., Armston, J.D., Disney, M., Jones, S.D., Suarez, L., Hill, M.J., Wilkes, P., Soto-Berelov, M., 2016. Quantifying the impact of woody material on leaf area index estimation from hemispherical photography using 3D canopy simulations. Agric. For. Meteorol. 226–227, 1–12. https://doi.org/10.1016/j.agrformet.2016.05.009.
Woodgate, W., Armston, J.D., Disney, M., Suarez, L., Jones, S.D., Hill, M.J., Wilkes, P., Soto-Berelov, M., 2017. Validating canopy clumping retrieval methods using hemispherical photography in a simulated Eucalypt forest. Agric. For. Meteorol. 247, 181–193. https://doi.org/10.1016/j.agrformet.2017.07.027.
Xie, Q., Dash, J., Huete, A., Jiang, A., Yin, G., Ding, Y., Peng, D., Hall, C.C., Brown, L., Shi, Y., Ye, H., Dong, Y., Huang, W., 2019. Retrieval of crop biophysical parameters from Sentinel-2 remote sensing imagery. Int. J. Appl. Earth Obs. Geoinf. 80, 187–195. https://doi.org/10.1016/j.jag.2019.04.019.
Xu, B., Li, J., Park, T., Liu, Q., Zeng, Y., Yin, G., Zhao, J., Fan, W., Yang, L., Knyazikhin, Y., Myneni, R.B., 2018. An integrated method for validating long-term leaf area index products using global networks of site-based measurements. Remote Sens. Environ. 209, 134–151. https://doi.org/10.1016/j.rse.2018.02.049.
Yan, K., Park, T., Chen, C., Xu, B., Song, W., Yang, B., Zeng, Y., Liu, Z., Yan, G., Knyazikhin, Y., Myneni, R.B., 2018. Generating global products of LAI and FPAR From SNPP-VIIRS data: theoretical background and implementation. IEEE Trans. Geosci. Remote Sens. 56, 2119–2137. https://doi.org/10.1109/TGRS.2017.2775247.
Yan, G., Hu, R., Luo, J., Weiss, M., Jiang, H., Mu, X., Xie, D., Zhang, W., 2019. Review of indirect optical measurements of leaf area index: recent advances, challenges, and perspectives. Agric. For. Meteorol. 265, 390–411. https://doi.org/10.1016/j.agrformet.2018.11.033.
Yan, K., Park, T., Yan, G., Chen, C., Yang, B., Liu, Z., Nemani, R., Knyazikhin, Y., Myneni, R., 2016a. Evaluation of MODIS LAI/FPAR product collection 6. Part 1: consistency and improvements. Remote Sens. 8, 359. https://doi.org/10.3390/rs8050359.
Yan, K., Park, T., Yan, G., Liu, Z., Yang, B., Chen, C., Nemani, R., Knyazikhin, Y., Myneni, R., 2016b. Evaluation of MODIS LAI/FPAR product collection 6. Part 2: validation and intercomparison. Remote Sens. 8, 460. https://doi.org/10.3390/rs8060460.
Yang, W., Tan, B., Huang, D., Rautiainen, M., Shabanov, N.V., Wang, Y., Privette, J.L., Huemmrich, K.F., Fensholt, R., Sandholt, I., Weiss, M., Ahl, D.E., Gower, S.T., Nemani, R.R., Knyazikhin, Y., Myneni, R.B., 2006. MODIS leaf area index products: from validation to algorithm improvement. IEEE Trans. Geosci. Remote Sens. 44, 1885–1898. https://doi.org/10.1109/TGRS.2006.871215.
Yin, G., Li, A., Jin, H., Zhao, W., Bian, J., Qu, Y., Zeng, Y., Xu, B., 2017. Derivation of temporally continuous LAI reference maps through combining the LAINet observation system with CACAO. Agric. For. Meteorol. 233, 209–221. https://doi.org/10.1016/j.agrformet.2016.11.267.